

RESEARCH ARTICLE

Open Access



Different amyloid β 42 preparations induce different cell death pathways in the model of SH-SY5Y neuroblastoma cells

Alp Yigit Özdemir¹, Kateřina Hofbauerová², Vladimír Kopecký Jr.², Jiří Novotný¹ and Vladimír Rudajev^{1*} 

*Correspondence:
rudajev@natur.cuni.cz

¹ Department of Physiology,
Faculty of Sciences, Charles
University, Viničná 7,
12844 Prague 2, Czech Republic

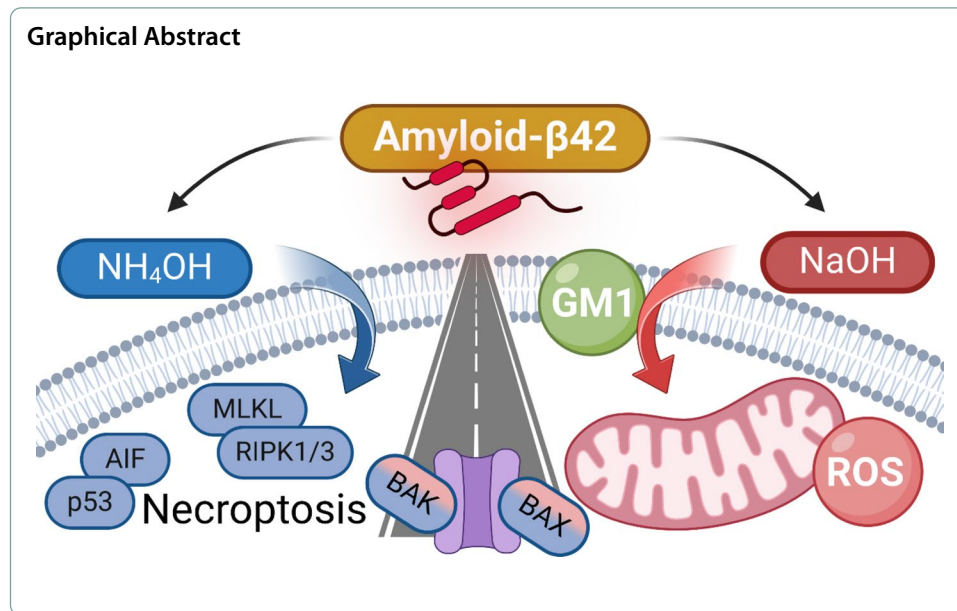
² Institute of Physics, Faculty
of Mathematics and Physics,
Charles University, Ke Karlovu 5,
12116 Prague 2, Czech Republic

Abstract

Amyloid β 42 (A β 42) plays a decisive role in the pathology of Alzheimer's disease. The A β 42 peptide can aggregate into various supramolecular structures, with oligomers being the most toxic form. However, different A β species that cause different effects have been described. Many cell death pathways can be activated in connection with A β action, including apoptosis, necroptosis, pyroptosis, oxidative stress, ferroptosis, alterations in mitophagy, autophagy, and endo/lysosomal functions. In this study, we used a model of differentiated SH-SY5Y cells and applied two different A β 42 preparations for 2 and 4 days. Although we found no difference in the shape and size of A β species prepared by two different methods (NaOH or NH₄OH for A β solubilization), we observed strong differences in their effects. Treatment of cells with NaOH-A β 42 mainly resulted in damage of mitochondrial function and increased production of reactive oxygen species, whereas application of NH₄OH-A β 42 induced necroptosis and first steps of apoptosis, but also caused an increase in protective Hsp27. Moreover, the two A β 42 preparations differed in the mechanism of interaction with the cells, with the effect of NaOH-A β 42 being dependent on monosialotetrahexosylganglioside (GM1) content, whereas the effect of NH₄OH-A β 42 was independent of GM1. This suggests that, although both preparations were similar in size, minor differences in secondary/tertiary structure are likely to strongly influence the resulting processes. Our work reveals, at least in part, one of the possible causes of the inconsistency in the data observed in different studies on A β -toxicity pathways.

Keywords: Amyloid β 42, Alzheimer's disease, Cell death, Apoptosis, Necroptosis, Reactive oxygen species, GM1





Introduction

Various neuronal death pathways have been described in association with Alzheimer's disease (AD). Apoptosis, necroptosis, reactive oxygen species (ROS)-induced damage (including ferroptosis), pyroptosis, mitochondrial malfunction, and fatal alterations in autophagy, mitophagy, or lysosomal functioning are induced by amyloid β ($A\beta$) [1].

Various $A\beta$ species differing in size and shape may induce distinct effects, but $A\beta_{42}$ oligomers represent the most toxic form [2–6]. Their size is estimated to be about 5–20 nm (>50 kDa), which corresponds to a composition ranging from a few to tens of monomers [7–13]. Different $A\beta$ aggregates show different behavior that also depends on cell type [4, 14]. Furthermore, $A\beta$ oligomers of similar molecular weight (MW) may differ in secondary, tertiary, and quaternary structure, all of which may affect $A\beta$ –cell interactions and consequential effects connected with toxicity [5, 15, 16]. The ability of $A\beta$ to induce cell death (CD) also depends on membrane composition, where various $A\beta$ receptors including ganglioside GM1 play a role [8, 17–23]. Therefore, the selection of an experimental model and appropriate $A\beta$ species is of principal importance, and it is not surprising that activation of different CD pathways has been described in association with $A\beta$ action. In the following section, we briefly describe the CD pathways that are related to AD.

Apoptosis: Some extracellular signals induce extrinsic apoptosis by activation of caspase 8 (Cas8) within the membrane death-inducing signalling complex. Activation of executioner Cas3 follows, which is an element common to both extrinsic and intrinsic apoptosis (reviewed in Refs. [24–26]). Intrinsic apoptosis is programmed CD initiated by various signals associated with enhanced ROS production, damage of DNA, endoplasmic reticulum (ER) stress, Ca^{2+} elevation, etc. The mitochondrion stays at the center of events: the proapoptotic inputs cause permeabilization of mitochondrial membranes, which leads to alteration in the inner membrane potential, decreased ATP production, and release of Ca^{2+} ions. Under cellular stress, BAK and BAX are released from antiapoptotic prosurvival proteins (e.g., Bcl-XL, Bcl-2) and

self-organize into the mitochondrial outer membrane pore (MOMP). Several factors are then released from mitochondria, including cytochrome c and apoptosis-inducing factor (AIF), which may lead to DNA damage and activation of Cas9 and executioner Cas3/7 [24, 26, 27]. Activated caspases cleave cellular proteins, leading to disruption of the plasma membrane (PM) and extracellular exposure of phosphatidylserine and CD. Caspase-independent apoptosis includes MOMP formation, DNA cleavage, and enhanced ROS production, but no activity of caspases [1, 28–32].

ROS-induced CD and ferroptosis: In ferroptosis, elevated iron levels increase the production of ROS, which cause lipid peroxidation, decreased functionality of antioxidant systems, and severe mitochondrial damage, all of which are associated with AD [33–38]. However, even A β 42 alone may induce ROS generation and CD, as shown in various models, including neuroblastoma SH-SY5Y cells [34, 39–44].

Necroptosis represents a programmed form of necrosis associated with organization of a necrosome—a complex composed of receptor-interacting protein kinases (RIPK) 1 and 3 and mixed lineage kinase domain-like pseudokinase (MLKL), whose activation by phosphorylation and oligomerization leads to permeabilization of PM and CD [26, 45–48]. *Pyroptosis* is associated with inflammation and thus strongly related to AD [26, 49]. The key structure is the inflammasome that can activate Cas1/11. Cas1 then cleaves gasdermin D, whose fragments create a pore in PM and cause necrosis (reviewed in Refs. [1, 50]).

In AD, often following A β action, the cellular degradative apparatuses are damaged at different levels and in many ways. *Lysosomal dysfunction* reflects the aggregation of A β , which induces membrane permeabilization, H⁺ leakage, release of cathepsins, accumulation of damaged proteins and mitochondria, and thus increased ROS production [1, 26, 51, 52]. Autophagy and mitophagy serve as important protective mechanisms, hence their disruption may also lead to CD. Both decreased and increased autophagy/mitophagy are connected with AD-related CD as a consequence of nonsufficient degradation of misfolded and aggregated proteins, or hyperactivated degradation of cytoplasmic components [26, 53–57].

The pathways of CD, including apoptosis, autophagy, mitophagy, or necroptosis, cross-talk directly or indirectly at multiple levels, complicating the ability to characterize specific processes [1, 48, 58–63]. Caspases may inhibit autophagy or necroptosis [27], and Cas8 or RIPK1 play roles in extrinsic and intrinsic apoptosis as well as necroptosis or inflammation [24–26, 31, 48, 64–66]. A β -induced apoptosis may affect inflammasome activation, but also inflammasome protein NLRP3 can activate Cas8 and induce apoptosis [16, 67]. Furthermore, by elevating ROS or cytosolic Ca²⁺ concentration, A β impairs many cellular functions [19, 68, 69]. Time course and subcellular localization of events, as well as a level of stress, also determine the direction toward a particular CD [27, 58–61, 70, 71]. Finally, several processes may occur simultaneously, as was shown in rats, where necroptosis and ferroptosis were activated, but also Cas8 was upregulated. There, ferroptosis was upstream of necroptosis, which indicates the complexity of A β effects on cell survival [72]. All interactions between CD pathways strongly depend on cellular context as well as on the A β species and the selected model. Also, some types of CD may represent attractors for different entries; e.g., DNA damage, ROS elevation, ER stress,

energy deficiency, mitochondrial damage, and some extrinsic imputes may all result in apoptosis.

In the present study, we focused on the characterization of the CD pathways induced by two distinct A β 42 oligomeric aggregates, viz. NaOH-A β 42 and NH₄OH-A β 42 preparations. We used a model of differentiated neuroblastoma SH-SY5Y cells and tried to describe the effects elicited by distinct A β oligomers. We found significant differences at several levels that emphasize the complexity of A β action and its dependence on the precise character of the A β species.

Materials and methods

Materials

Amyloid beta 1–42 (CAS no. 107761-42-2) was obtained from Bachem AG (Switzerland). Trypan-Blue (CAS no. 72-57-1), Dulbecco's modified Eagle's medium—high glucose (D6429-500 ml), retinoic acid (CAS Number: 302-79-4), antibiotic antimycotic solution (100 \times), 1,1,1,3,3,3-hexafluoro-2-propanol (HFIP) (CAS no. 920-66-1), stabilized A5955, Acridine Orange (AO) hemi(zinc chloride) salt (CAS no. 10127–02-3), propidium iodide (PI) solution (CAS no. 25535-16-4), 2',7'-dichlorodihydrofluorescein diacetate (DCF-DA) (CAS no. 2044-85-1), malondialdehyde bis(dimethyl acetal) (CAS no. 102–52-3), trichloroacetic acid (TCA) (CAS no. 76-03-9), 2-thiobarbituric acid (TBA) (CAS no. 504-17-6), cholera toxin B subunit (C3741), dimethyl sulfoxide (DMSO) (CAS no. 67–68-5), trypsin–EDTA solution (T4174), sodium hydroxide (CAS no. 1310-73-2), ammonia solution 28–30% (CAS no. 1336-21-6), Ponceau S (CAS no. 6226-79-5), ammonium persulfate (APS) (CAS no. 7727-54-0), Complete™, Mini Protease Inhibitor Cocktail (11,836,153,001), PhosSTOP (PHOSS-RO), sodium carbonate (CAS no. 497-19-8), glycerol (CAS no. 56-81-5), sodium tartrate dihydrate (CAS no. 6106-24-7), copper(II) sulfate pentahydrate (CAS no. 7758-99-8), ethanol (CAS no. 64-17-5), sodium chloride (CAS no. 7647-14-5), bovine serum albumin (BSA) (CAS no. 9048-46-8), anti-amyloid- β (oligomer) antibody, clone F11G3 antibody (MABN1839), and thiazolyl blue tetrazolium bromide (CAS no. 298-93-1) were purchased from Merck–Sigma-Aldrich (Germany). BAK (sc-517390), caspase 3 (sc-7148), caspase 12 (sc-5627), AIF (sc-13116), ATF6 α (sc-166659), SOD-2 (sc-30080), F₁-ATPase (sc-55597), spectrin α II (sc-48382), HSP70 (sc-1060), HSP90 (sc-13119), HSP27 (sc-101699), MLKL (sc-293201), RIP3 (sc-374639), β -amyloid antibody (B-4) (sc-28365), rabbit anti-mouse IgG-HRP (sc-358914), mouse anti-rabbit IgG-HRP (sc-2357), and mouse anti-goat IgG-HRP (sc-2354) antibodies were purchased from Santa Cruz Biotechnology (Germany). BAX (ab32503), p53 (A19585), mt-TFA (ab131607), gasdermin D, and phospho-MLKL-T357/S358/S360 (AP0949) antibodies were purchased from ABclonal (Germany). Glycine (CAS no. 56–40-6), Tween® 20 (CAS no. 9005-64-5), bromophenol blue·Na salt (CAS no. 34725-61-6), acrylamide/bis Solution (10,688.01), and Tris(hydroxymethyl)aminomethane (CAS no. 77-86-1) were obtained from SERVA (Germany). Fetal bovine serum (cat. no. 10270106), Hoechst 33,258, pentahydrate (bis-benzimide) (cat. no. H3569), MitoTracker™ dyes for mitochondria labeling (cat. no. M7514), MitoTracker™ dyes for mitochondria labeling (cat. no. M7512), SuperSignal™ West Femto maximum sensitivity substrate (cat. no. 34095), and TEMED (N,N,N',N'-tetramethyl-ethylenediamine) (cat. no. 17919) were purchased from ThermoFisher Scientific (Germany). Annexin V binding

buffer (10×) and Annexin V conjugated to Dyomix 647 were purchased from Exbio (Czechia). Premium Western blotting membranes were purchased from Amersham™ Protran® (NJ, USA). Phospho-RIP3 (Ser232) antibody (#AF7443) was purchased from SVEN BioLabs s.r.o. (Czechia). PARP1 polyclonal antibody (cat. no. E-AB-16025) was purchased from Elabscience (USA).

Cell culture and differentiation of SH-SY5Y cells

Human neuroblastoma SH-SY5Y cells (ATCC® CRL-2266™) were incubated in the Dulbecco's modified Eagle's medium—high glucose (DMEM-HG) with 10% fetal bovine serum (FBS) and 1% 100× penicillin/streptomycin (P/S) before differentiation. Then, they differentiated for 5–11 days in the differentiation medium (DMEM-HG, 1% FBS, 1% P/S, 100 μM retinoic acid). After differentiation, the expression levels of synaptophysin (Syp) and tyrosine hydroxylase (TH), which are expressed in mature neurons, increased. The differentiated cells were treated with different concentrations of Aβ oligomers for 2 or 4 days, and, in the case of GM1 manipulation, we applied (+)-D-threo-PDMP (*N*-[(1*R*,2*R*)-2-hydroxy-1-(4-morpholinylmethyl)-2-phenylethyl]-decanamide, D-PDMP) (Cayman Chemical, MI, USA).

Amyloid-β oligomerization

Aβ was oligomerized using NaOH and NH₄OH as described before [73–76]. Initially, Aβ was dissolved in 1,1,1,3,3,3-hexafluoro-2-propanol (HFIP). HFIP is widely used as an agent that solubilizes Aβ into monomers by disrupting noncovalent interaction between Aβ peptides. After HFIP solubilization, the samples were subjected to overnight evaporation. Aliquots of 100 μg were frozen at –20 °C. Before application, the HFIP solubilization was repeated and a 1-h vacuum evaporation step was added. The resulting pellets were dissolved in either 10 mM NaOH or 10% NH₄OH (2, 85 M) solution. After another drying process, the pellets were frozen (–20 °C) for later use or dissolved in 2 μl dimethyl sulfoxide (DMSO) and then diluted with phosphate-buffered saline (PBS) (137 mM NaCl, 2.7 mM KCl, 10 mM Na₂HPO₄, 1.8 mM KH₂PO₄, pH 7.4) to a final concentration of 1 μg/μl (451 μM). Aβ in PBS was frozen (–20 °C, for a maximum of 1 month) or used immediately.

Dynamic light scattering

Dynamic light scattering (DLS) measurements were performed at a constant temperature of 20 °C on a Zetasizer Nano ZS (Malvern Instruments, UK) equipped with a He–Ne laser with a wavelength of 633 nm. Protein samples (dissolved in PBS buffer, 1 mg/ml) were centrifuged for 5 min, 20,000 revolutions, cooling at 10 °C to remove dust particles before measurement. Aβ₄₂ were measured in a 40 μL 3×3 mm quartz cuvette recommended by the manufacturer (Hellma Analytics, Germany). Each sample was measured in two series of ten runs. The resulting DLS data are given as averages of individual investigated values. The results were processed using the original Zetasizer 6.2 software (Malvern Instruments, Great Britain).

Atomic force microscopy

A β 42 samples were dissolved in PBS buffer at a concentration of 0.01 mg/ml. Peptide-mica samples for atomic force microscopy (AFM) were prepared in the standard following way [77]: Solutions of amyloid were adsorbed on freshly cleaved muscovite mica (V1 quality, Electron Microscopy Sciences, USA) for 20 min. Then, the excessive liquid sample was removed and the mica was heated up to 60 °C to avoid the formation of the coffee ring effect [78, 79] and pattern formation [80] and subsequent high-density induced fibrils formation. Finally, the mica was completely rinsed with ultrapure water and rapidly dried at 60 °C. AFM imaging was performed in contact mode with combined Raman/AFM/SNOM micro-spectrometer alpha300 RSA (WITec, Germany) using silicon AFM Arrow cantilevers (0.2 N/m, 14 kHz, WITec, Germany). The data were subsequently analyzed and images were treated using Project SIX Plus 6.0 software (WITec, Germany).

Determination of cell viability

Cell viability was measured with the 3-(4,5-dimethylthiazol-2-yl)-2,5-diphenyltetrazolium bromide (MTT) and Trypan blue (TB) assays. The MTT test is a calorimetric cell viability assay that determines the number of living cells by analyzing the formazan crystals generated by viable cells [81]. Cells were seeded to 96-well plates at a density of 7500 cells/well for differentiation and treatment. For the MTT assay, as detailed in earlier studies [81, 82], cells were washed with PBS after removing the culture medium. Cells were incubated with a serum-free medium containing 10% MTT solution, for 4 h at 37 °C with 5% CO₂. DMSO was used to dissolve the formazan crystals, creating a violet-like color. Absorbance at 570 nm was measured using a Biotek Synergy HT multi-mode microplate reader (Marshall Scientific, NH, USA). The percentage of cell viability compared with the control group was determined using the measured absorbance values and compared statistically with each other.

TB is a dye that selectively stains dead cells. Healthy cells possess intact cell membranes, which prevent the dye from entering the cell. In contrast, damaged or dead cells have compromised membranes, allowing TB to penetrate and stain them [83, 84]. Cells were seeded to 25 cm² flasks at a density of 2×10^6 cells/flask. After the treatment, cells were washed with PBS, trypsinised, and centrifuged. The resulting cell pellet was then resuspended in PBS and incubated at room temperature with 0.4% TB dye solution for 5 min. Subsequently, the mixture was examined under a microscope, and both viable (unstained) and nonviable (stained) cells were counted to assess cell viability accurately.

Assessment of oxidative stress and mitochondrial damage

The DCF-DA assay was employed to quantify the level of ROS and oxidative stress [42]. This assay relies on the diffusion of DCF-DA into cells, where cellular esterases catalyze its deacetylation, yielding a nonfluorescent molecule. Upon oxidation by ROS, this molecule is converted to 2',7'-dichlorofluorescein (DCF), a fluorescent compound. The fluorescence of DCF can be detected and quantified using fluorescence spectroscopy at wavelengths of 485 nm for excitation and 535 nm for emission [85]. Cells were seeded on 96-well plates and, after A β treatment, incubated with DCF-DA solution for 30 min

at 37 °C/5% CO₂. Following the incubation period, the DCF-DA solution was removed, and the cells were further washed with PBS. Imaging was performed using an inverted fluorescence microscope AIF 5114i-T (ARSENAL, Czechia). The acquired images were analyzed using ImageJ software (National Institutes of Health, USA).

The thiobarbituric acid reactive substances (TBARS) assay is based on the principle of measuring the end-products of lipid peroxidation, primarily malondialdehyde (MDA) and related substances. Under acidic and high-temperature conditions, MDA reacts with thiobarbituric acid (TBA) to form a pink-colored complex. The intensity of this color is proportional to the concentration of MDA in the sample and was measured spectrophotometrically at around 532–535 nm. Calibration with known MDA standards allows for the quantification of lipid peroxidation, providing a valuable tool to assess oxidative damage to lipids in biological samples [85]. To investigate the concentration of malondialdehyde (MDA), cells were harvested into an ice-cold homogenizing buffer and proteins were extracted. Subsequently, the collected proteins underwent treatment with thiobarbituric acid (TBA) and trichloroacetic acid (TCA). The MDA levels in the samples were then quantified using a Biotek Synergy HT multi-mode microplate reader (Marshall Scientific, NH, USA) with fluorescence excitation at 540/25 nm and emission at 590/35 nm. Statistical methods were employed to compare the measured MDA levels among the different samples.

Mitotracker Green is a selective probe that labels mitochondria by binding to mitochondrial proteins and aggregating in the mitochondrial matrix. Importantly, the reaction of Mitotracker Green remains unaffected by changes in the mitochondrial membrane potential. This feature makes it a valuable tool for assessing mitochondrial mass, as it provides a reliable measure regardless of variations in membrane potential [87, 88]. MitoTracker Red, however, is a fluorescent dye that specifically targets mitochondria and is used to measure mitochondrial membrane potential. This dye can only enter mitochondria with a negatively charged and polarized inner membrane, which is indicative of proper mitochondrial function. Thus, MitoTracker Red serves as a useful agent for assessing mitochondrial health and energy production [88, 89].

To assess mitochondrial mass and membrane potential, as described before ([90]), cells were washed with PBS after removing the culture medium and incubated with either 20 nM MitoTracker Green or 20 nM MitoTracker Red. After the incubation, cells were trypsinized and analyzed using flow cytometry with 488 ex 525/50 bp filter for Mitotracker Green and 561 ex 586/15 bp filter for Mitotracker Red by LSRII flow cytometer (BD Biosciences, USA). All obtained data were processed using Kaluza Analysis 2.1 software (Beckman Coulter, USA).

Determination of the extent of apoptosis and necrosis

The Acridine Orange (AO) and propidium iodide (PI) assay is a widely used method to distinguish between apoptotic and necrotic cells on the basis of changes in nuclear morphology and membrane integrity. AO, a nucleic acid-specific dye, can penetrate the membranes of both living and early apoptotic cells, causing their nuclei to emit bright green fluorescence with intact structures. In contrast, PI is impermeable to intact cell membranes but can penetrate the damaged membranes of late apoptotic and necrotic cells, causing their nuclei to emit red fluorescence. Therefore, uniform green

fluorescence characterizes living cells with an organized structure. Early apoptotic cells are distinguished by bright-green areas of chromatin condensation, while late apoptotic cells exhibit dense orange chromatin condensation. Necrotic cells are identified by their orange fluorescence and intact nuclei. By using a fluorescence microscope, the AO/PI assay enables the quantification of apoptotic and necrotic cells [91–93]. After cultivation in 25 cm² flasks, the cell culture was washed with PBS and the cells were stained with a 1:1 mixture of AO (final concentration: 0.5 mg/1 mg) and PI (final concentration: 0.5 mg/1 mg) for 1 min. After removing the dye, cells were washed twice with PBS. Imaging was conducted using an inverted fluorescence microscope AIF 5114i-T (ARSENAL, Czechia) and apoptotic and necrotic cells were quantified using ImageJ (National Institutes of Health, USA).

Annexin V is an agent that selectively binds to phosphatidylserine (PS), a membrane lipid exposed on the outer leaflet of apoptotic cell membranes. Concurrently, Hoechst 33,258, a DNA-binding dye, stains the nuclei of cells, aiding in the identification of morphological changes associated with apoptosis and necrosis. By utilizing Hoechst in combination with Annexin V, this staining approach allows for the distinction between cells undergoing apoptosis, where Annexin V binds to PS, and those with disrupted cell membranes characteristic of necrosis. The combined use of Annexin V and Hoechst enhances the specificity of detecting different cell death modalities [90, 94–96].

As described in a previous study [90], cells were harvested and centrifuged. After centrifugation, cells were resuspended in annexin binding buffer (ABB), and Annexin V conjugated to Dyomix 647 was added at a final concentration of 1%. The cells were then incubated on ice in the dark for 30 min. After incubation, cells were centrifuged again and resuspended in 150 µL of ABB. Ten minutes before measurement, Hoechst 33,258 was added to the cells at a final concentration of 1 µg/mL. Flow cytometric analysis was conducted on an LSRII flow cytometer (BD Biosciences, USA) using the recommended optical configurations. Annexin V–Dyomix 647 was detected using the 640 ex 670/30 bp filter, while Hoechst was measured using the 405 ex 450/40 bp filter. Data obtained from the FC data were processed using Kaluza Analysis 2.1 software (Beckman Coulter, USA).

Western blotting

The analysis of protein levels after treatment was conducted using Western blotting. As described before [85, 97], cells were harvested, centrifuged, and resuspended in TMES buffer containing a Complete Protease Inhibitor Cocktail. The cell suspension was subjected to 2×10 s, 50% intensity sonication using a Bandelin Sonopuls HD 2070 ultrasonic homogenizer (BANDELIN electronic, Germany) for lysis. Samples for detection of phosphorylated RIPK3 and MLKL were lysed using radioimmunoprecipitation assay (RIPA) buffer in the presence of a phosphatase inhibitor (PhosSTOP). The protein separation was done with electrophoresis using 10–15% separation sodium dodecyl sulfate (SDS)-polyacrylamide gel electrophoresis (PAGE) gel. For each sample, 1 µg/µl protein in Laemmli buffer was loaded (20 µg per lane) and separated by size using an electrophoresis apparatus (Bio-Rad Laboratories, Hercules, CA, USA) at 200 V for 45 min. After separation, proteins were subsequently transferred onto nitrocellulose membranes. Nonspecific binding sites were blocked with

5% dry milk dissolved in TBS-Tween buffer. The target proteins were identified with specific antibodies and visualized with the HRP-labelled secondary antibody using the West Femto maximum sensitivity substrate. The resulting images were analyzed using ImageJ and Image Lab, and the data were normalized by β -actin protein expression.

Statistics

The statistical comparisons were conducted among the results obtained from 3–6 independent experiments. The comparison was performed using one-way analysis of variance (ANOVA), followed by the Tukey post test. The observed differences were determined based on their significance levels determined by *p*-values.

Results

Preparation of A β 42 oligomers

We prepared A β 42 oligomers by dissolving the dried peptide in HFIP (see “Methods”). As mainly large amyloid aggregates (measured by DLS) were obtained, we repeated the

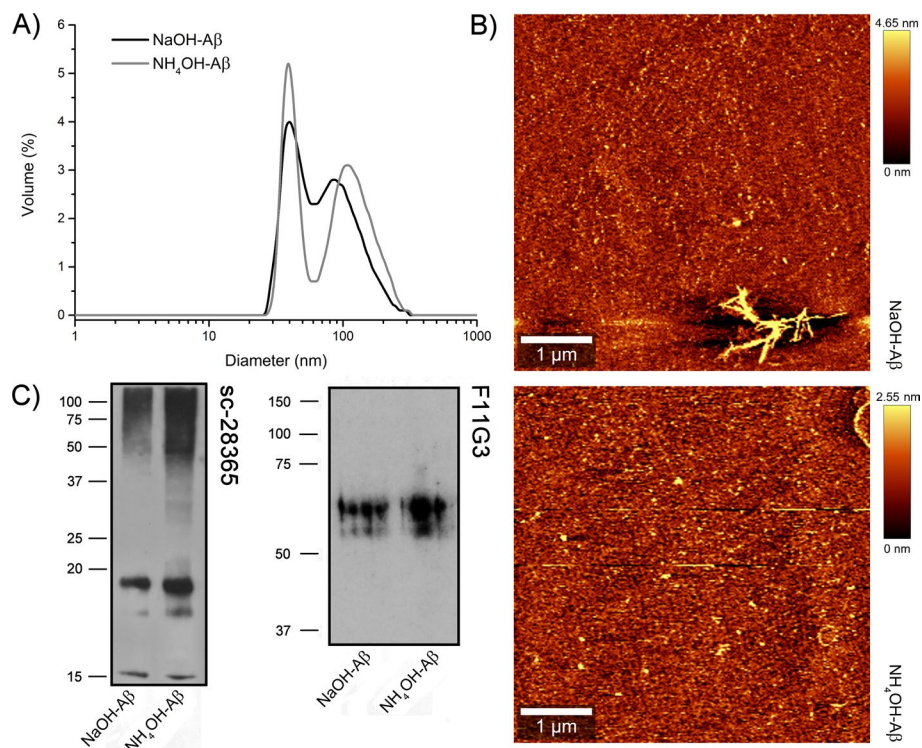


Fig. 1 Structural and size characterization of A β 42 oligomers by (A) dynamic light scattering, (B) atomic force microscopy, and (C) western blotting using antibodies against A β 42. A Particle size distribution of NaOH-A β 42 and NH₄OH-A β 42 preparation aggregates given by their volumes (amounts) derived from intensity measurements of DLS. B Representative figures from AFM depicting 5 x 5 μ m regions where dominantly small globular particles are observable in both NaOH-A β 42 (above) and NH₄OH-A β 42 preparations. Slightly bigger particles are rarely observable as well. Clusters of growing A β 42 fibrils are observable in bottom left/top right for NaOH-A β 42/NH₄OH-A β 42 preparations. (Such fibrils were removed from the samples by filtration). C Western blots of A β 42 oligomers. 10 μ g of NaOH-A β 42 or NH₄OH-A β 42 preparation were loaded on SDS-PAGE. Two different antibodies against A β 42 were used. Sc-28365 antibodies recognized different amyloid aggregates with strong band corresponding to A β 42 tetramer (< 20 kDa) and weaker band corresponding to the trimer (~ 15 kDa). The use of antibodies F11G3 developed against A β oligomers showed only two bands with MW of 64 and 57 kDa corresponding to ~ 12/14-mers

HFIP solubilization with vacuum evaporation step, and then we solubilized the pellet with agents preventing A β aggregation, viz. NaOH or NH₄OH, respectively [73–76]. DLS measurements indicated that NaOH-A β 42 samples were somewhat smaller than NH₄OH-A β 42 preparations; however, later experiments did not confirm significant size differences (Fig. 1A). On the contrary, there was a dominant representation of smaller oligomers (30–50 nm, with average size 41 nm) in the NH₄OH-A β 42 samples, but the majority of the scattered signal corresponded to less populated larger particle sizes of 80–110 nm in both preparations. We thus suppose that the majority of oligomers were composed of >10 monomers (based on dimension given by Ref. [98]). However, based on DLS spectra, we were not able to distinguish the exact shape, and whether globular or fibrillar oligomers prevail.

In the following step, we used AFM for closer approximation (Fig. 1B). In a general view, it can be stated that both types of samples showed a dominant proportion of small parts of globular shape. The NH₄OH-A β 42 aggregates appeared a little higher, which could be due to a greater accumulation of amyloid subunits. In our study, the average height of the aggregates was 4 nm, and their width ranged from roughly 60 to 80 nm, which corresponds to the organization of maximally 20 amyloid peptides in a globular formation (compared with dimensions given in Ref. [98]). However, the detected size will be systematically larger because we did not use high-resolution AFM. This was also confirmed by the comparison with DLS, because the width of the size interval was preserved; only a shift to larger dimensions has occurred. So, we can assume that the size of A β 42 will be slightly smaller, corresponding to DLS.

Both AFM and DLS did not show a marked size difference between the NaOH-A β 42 and NH₄OH-A β 42 preparations. However, we cannot exclude that both populations differed in the representation profile of the oligomers. For a more detailed view, we analyzed NaOH-A β 42 and NH₄-A β 42 aggregates using western blotting. We used two different antibodies against A β 42, and none of them showed a marked difference in both NaOH-A β 42 and NH₄-A β 42 preparations. As shown in Fig. 1C, antibodies directed against A β 42 (sc-28365) gave identical signals corresponding mainly to the tetramer (below 20 kDa) but also to the probable trimer (15 kDa). Because we also obtained an equivocal signal in the region corresponding to MW above 50 kDa, we used specific antibodies against the oligomeric form of A β . It can be seen from the figure that these antibodies distinguished two clear bands, the stronger one corresponding to MW of 64 kDa, and the weaker one to 57 kDa. These aggregates thus represented amyloid species composed of ~12/14 monomers, which is in accordance with data from DLS and AFM.

Amyloid β 42 toxicity

The SH-SY5Y cell line is a human neuroblastoma cell line that can be differentiated into neuron-like cells, making them suitable for studying the mechanisms of neurodegenerative disorders and testing potential therapeutic interventions [76, 84, 99–101]. We used differentiated SH-SY5Y cells as a model for A β 42 toxicity. Differentiation was achieved for 7 days by using 100 μ M retinoic acid (see “Methods”) and was verified by measuring protein markers (synaptophysin, tyrosine hydroxylase) on immunoblot (Supplementary Fig. S1).

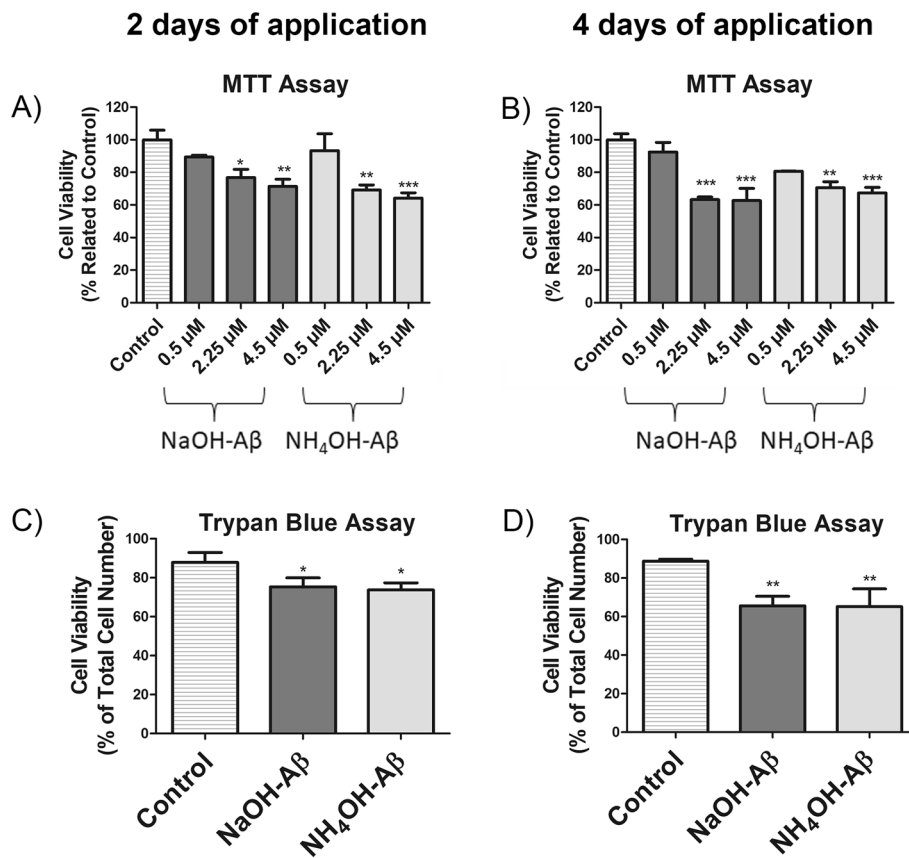


Fig. 2 Cell viability assessment. Quantitative assessment of cellular viability following treatment with NaOH and NH₄OH-Aβ₄₂ applications via MTT (**A, B**) and TB (**C, D**) assays. **A** MTT analysis after 2 days revealed a significant decrease in viability with both 2.25 μM NaOH-Aβ₄₂ ($n=3$, 76.78%, $p=0.052$) and NH₄OH-Aβ₄₂ ($n=3$, 69.15%, $p=0.007$), as well as with 4.5 μM NaOH-Aβ₄₂ ($n=3$, 71.37%, $p=0.013$) and NH₄OH-Aβ₄₂ ($n=3$, 64.19%, $p=0.002$). **B** MTT analysis after 4 days showed a further decrease in viability with 2.25 μM NaOH-Aβ₄₂ ($n=4$, 63.22%, $p=0.0002$) and NH₄OH-Aβ₄₂ ($n=4$, 70.60%, $p=0.0019$), or with 4.5 μM NaOH-Aβ₄₂ ($n=4$, 62.67%, $p=0.002$) and NH₄OH-Aβ₄₂ ($n=4$, 67.35%, $p=0.0007$). The TB assay confirmed reduced viability after 2 days (**C**) with 2.25 μM NaOH-Aβ₄₂ ($n=3$, 75.35%, $p=0.033$) and NH₄OH-Aβ₄₂ ($n=3$, 73.67%, $p=0.019$) or after 4 days (**D**) with 2.25 μM NaOH-Aβ₄₂ ($n=3$, 65.64%, $p=0.019$) and NH₄OH-Aβ₄₂ ($n=3$, 65.19%, $p=0.007$). Statistical significance level versus untreated samples: * $p\leq 0.05$, ** $p\leq 0.01$, *** $p\leq 0.001$

After incubation with Aβ₄₂, we monitored toxicity toward differentiated SH-SY5Y cells by the MTT test, which is widely used for measurement of cell viability [39, 41, 54, 75, 102–104]. We applied three different concentrations of both NaOH-Aβ₄₂ and NH₄OH-Aβ₄₂ preparations. Figure 2A shows that both types of Aβ₄₂ aggregates reduced the viability of SH-SY5Y cells to below 75% at concentrations of 2.25 and 4.5 μM. We chose the 2,25 μM Aβ₄₂ as a working concentration because it was the lowest concentration with a significant toxic effect.

Incubations with Aβ longer than 2 days are relatively rare [84, 100], while short-term treatments (hours to 2 days) are more common [16, 37, 39, 41, 44, 54, 69, 75, 102, 103, 105]. However, the processes induced by the Aβ are dynamic and may change over time. Therefore, in our model of differentiated SH-SY5Y cells, we compared 2- and 4-day applications of Aβ₄₂ preparations. As shown in Fig. 2B, after 4 days of Aβ

treatment, the toxic effect of the amyloid measured by the MTT test was accentuated (Fig. 2B).

The TB assay, which is used for quantifying dead cells [83, 84], confirmed our results with 2.25 μ M A β obtained by MTT test. The percentage of viable cells in groups treated with NaOH-A β 42 and NH₄OH-A β 42 was determined to be 75.35% and 73.67% after 2 days of application, and 65.64% and 65.19% after 4 days of application, respectively (Fig. 2C, D). We also excluded the toxicity of DMSO and NH₄OH applied without A β (Supplementary Fig. S2).

Amyloid β 42-induced cell death: necrotic or apoptotic?

We confirmed the toxicity of both A β 42 preparations by measuring the level of p38, which was elevated after 4-day treatment (Supplementary Fig. S3). Activation of the ERK/p38 MAPK pathway is known to be connected with A β action [41, 44]. As we observed the toxicity of A β 42 in our model, we asked the question of whether the cell death (CD) was necrotic or apoptotic. In search for the answer, we analyzed our samples by flow cytometry (FC). In accordance with the MTT and TB assay, an elevated number of dead cells was recorded. The Hoechst 33,258 dye is not able to enter healthy cells, but it can permeate disturbed membranes of necrotic cells [90, 95]. In our experiments, we observed an increase in the number of necrotic cells by ~40–150% during both the 2- and 4-day applications of NaOH- and NH₄OH-A β preparations. On the other hand, annexin labeling showed no apoptosis to be underway in both preparations and in both time courses. However, in the 4-day application of the NH₄OH-A β 42, the number of apoptotic cells nonsignificantly increased, indicating the possible initiation of apoptosis (Fig. 3A).

The use of Acridine Orange and propidium iodide (AO/PI) as dyes, which are differentially incorporated into cells, also enables the monitoring of necrosis and apoptosis [91–93]. As shown in Fig. 3B, the results are similar to those from flow cytometry. We can again observe more than 150% increased number of necrotic cells (dark orange/red color) and, in the case of NH₄OH-A β 42 treated SH-SY5Y cells, also a slightly elevated number of apoptotic cells (bright-green nucleus with orange markings). We thus can conclude that, while both preparations of A β 42 are toxic and cause necrosis of the differentiated SH-SY5Y cells, in 4-day application of NH₄OH-A β 42, apoptosis may also be involved, but only to a small extent.

Apoptosis

Previous experiments were aimed at later stages of apoptosis connected with PM remodeling. To monitor apoptosis in more detail, we detected selected apoptotic markers connected with different stages of the process. As a hallmark of apoptosis, the activation of executioner caspases including Cas3 is a characteristic event. However, in all our experiments, no Cas3 level elevation or cleavage was detected (Fig. 4A). This result is in accordance with data from FC and AO/PI measurements, where no apoptosis was detected except in the NH₄OH-A β 42 4-day group, where a small portion of apoptotic cells was present.

In caspase-independent apoptosis [1, 28–32], BAX and BAK proteins self-organize into the MOMP through which proapoptotic elements release mitochondria, including

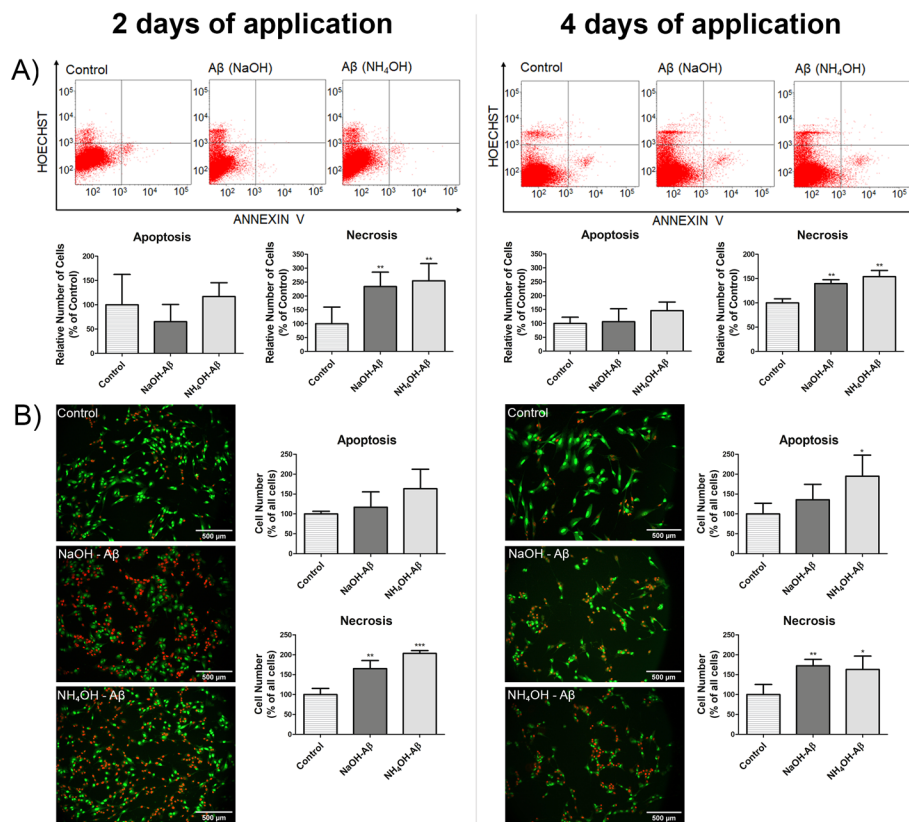


Fig. 3 Assessment of apoptosis and necrosis. **A** Using flow cytometry, Annexin V/Hoechst staining revealed no significant change in apoptosis levels, but a notable increase in necrosis levels following 2 and 4 days of application of both NaOH-Aβ ($n=3$, 139.67%, $p=0.00312$; $n=5$, 233.84%, $p=0.00879$, respectively) and NH₄OH-Aβ ($n=3$, 154.081%, $p=0.00042$; $n=5$, 254.34%, $p=0.00327$, respectively) preparations. **B** Results of the AO/PI assay (fluorescence microscopy) reflected these findings and showed an increased level of necrosis after 2 days (165,29%, $n=3$, $p=0.00472$ with NaOH-Aβ42; 203,39%, $n=3$, $p=0.00041$ with NH₄OH-Aβ42) and 4 days (172,24%, $n=4$, $p=0.00648$ with NaOH-Aβ42; 163,02%, $n=4$, $p=0.01511$ with NH₄OH-Aβ42). Additionally, NH₄OH-Aβ42 treatment led to a significant elevation in the number of apoptotic cells (194.82%, $n=4$, $p=0.01847$). Statistical significance level versus untreated samples: * $p \leq 0.05$, ** $p \leq 0.01$, *** $p \leq 0.001$

(See figure on next page.)

Fig. 4 Differential modulation of apoptosis and ER stress response pathways by application of NaOH-Aβ42 and NH₄OH-Aβ42. **A** Western blot analysis revealed changes in protein expression levels after 2 and 4 days of peptide treatment. BAX and BAK levels increased significantly after 2 days in NH₄OH-Aβ42-treated samples (172.69%, $n=3$, $p=0.00161$ and 140.78%, $n=3$, $p=0.00029$, respectively), while after 4 days, elevation was observed in both NaOH-Aβ (208.11%, $n=3$, $p=0.03325$ and 128.61%, $n=3$, $p=0.01048$, respectively) and NH₄OH-Aβ (202.70%, $n=3$, $p=0.04082$ and 124.78%, $n=3$, $p=0.02408$, respectively) samples. AIF levels significantly increased only after 4 days of NH₄OH-Aβ treatment (130.18%, $n=3$, $p=0.00651$), along with elevated p53 expression at both time points (151.78%, $n=5$, $p=0.01013$ after 2 days and 128.80%, $n=4$, $p=0.03613$ after 4 days). **B** ATF6α levels showed a consistent elevation in all preparations, with a significant increase observed after 2 days with NaOH-Aβ42 (172.73%, $n=3$, $p=0.00849$) and NH₄OH-Aβ42 (156.94%, $n=3$, $p=0.02558$), and after 4 days with NaOH-Aβ42 (137.77%, $n=3$, $p=0.02398$) and NH₄OH-Aβ42 (148.07%, $n=3$, $p=0.00803$). After 2 days, a significant increase in Cas12 levels was observed only with NH₄OH-Aβ42 (156.96%, $n=3$, $p=0.03186$), while after 4 days of treatment, Cas12 levels increased markedly with both NaOH-Aβ42 (160.92%, $n=3$, $p=0.03835$) and NH₄OH-Aβ42 (206.60%, $n=3$, $p=0.00291$). Statistical significance level versus untreated samples: * $p \leq 0.05$, ** $p \leq 0.01$, *** $p \leq 0.001$

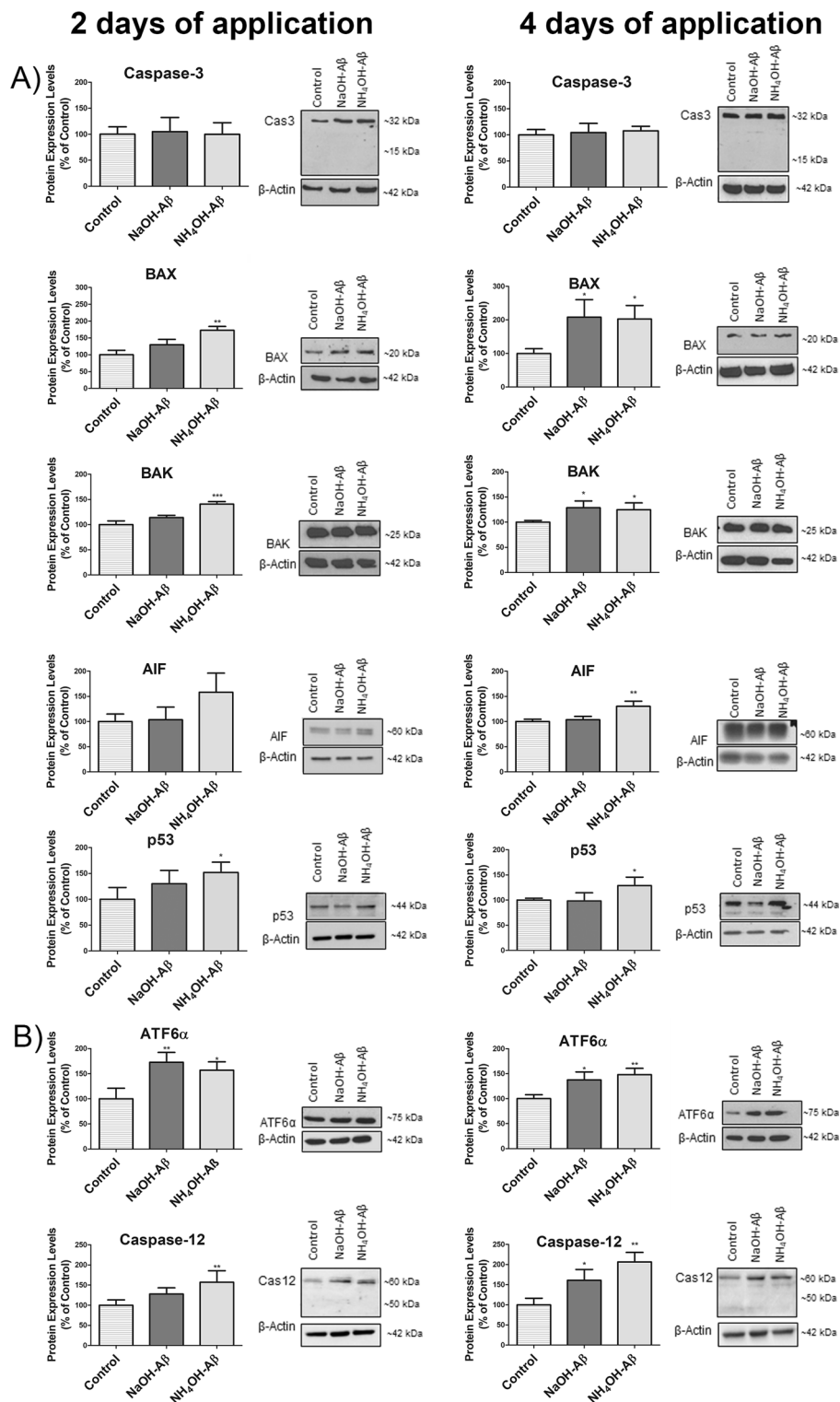


Fig. 4 (See legend on previous page.)

the AIF. In our model, 2-day treatment led to an elevation of BAX and BAK only in the $\text{NH}_4\text{OH-A}\beta_{42}$ preparation, to 172.69% and 140.78%, respectively. However, after 4 days of $\text{A}\beta_{42}$ application, they were elevated in both the NaOH- and $\text{NH}_4\text{OH-A}\beta_{42}$ samples (more than 200% in BAX and more than 120% in BAK). On the other hand, AIF significantly increased only in the 4-day $\text{NH}_4\text{OH-A}\beta_{42}$ application, for 130%, where p53, a transcription factor associated with apoptosis activation [106–108] was also elevated (after 2 days 151% and after 4 days 128%). As shown in Fig. 4A, p53 increased also in the 2-day $\text{NH}_4\text{OH-A}\beta_{42}$ application. Based on our data, we can conclude that, although apoptosis is not the main pathway of CD in our experiments, it appears that initial activation began, at least in the 4-day $\text{NH}_4\text{OH-A}\beta_{42}$ application.

ER stress may serve as one of many entry sites to CD. We analyzed two important markers of ER stress, ATF6 α and Cas12. Figure 4B shows that the amount of ATF6 α increased after 2 days of treatment in both preparations, to more than 140%. Similar data were obtained for 4 days of application. However, at 2 days, the amount of Cas12 increased (156%) only after $\text{NH}_4\text{OH-A}\beta_{42}$ treatment, whereas no significant difference was detected after incubation with NaOH- $\text{A}\beta_{42}$. These data indicate ER-induced apoptosis, as also observed in the SH-SY5Y model [109, 110]. Thus, we can assume that both $\text{A}\beta$ species induced damage to the ER function to a similar extent.

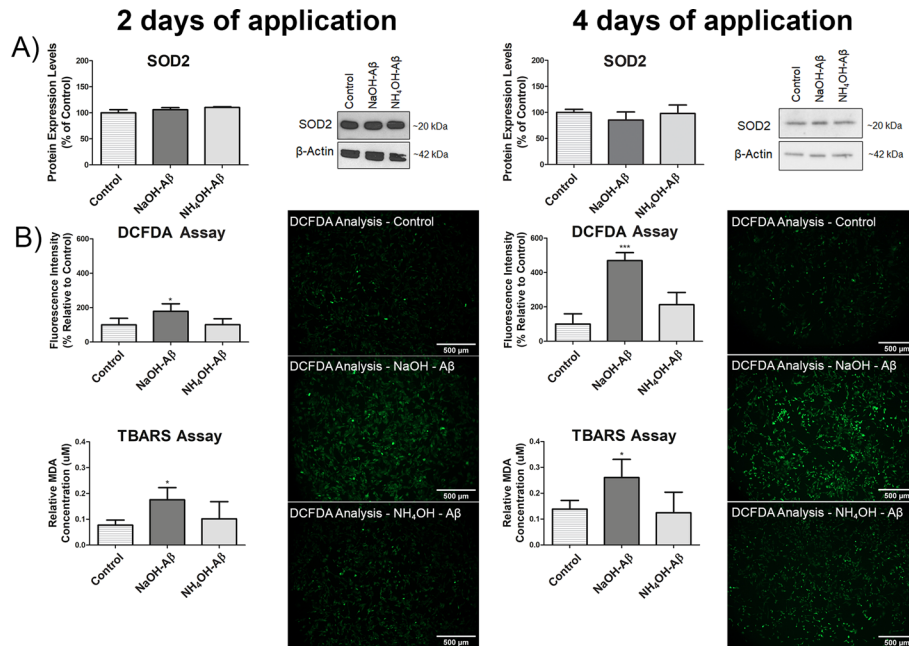


Fig. 5 Assessment of oxidative stress markers in response to NaOH- $\text{A}\beta_{42}$ and $\text{NH}_4\text{OH-A}\beta_{42}$ treatment. **A** SOD2 levels remained unchanged following 2- and 4-day application of both peptide preparations ($n = 3$). **B** DCFDA and TBARS assay to evaluate oxidative stress. DCFDA assay reveals a significant increase in fluorescence signal only in NaOH- $\text{A}\beta_{42}$ -treated cells after 2 days (178.57%, $n = 4$, $p = 0.0399$) and 4 days (469.10%, $n = 3$, $p = 0.00018$) of exposure, while no elevation is observed in $\text{NH}_4\text{OH-A}\beta_{42}$ -treated cells. TBARS assay demonstrates a consistent increase in malondialdehyde (MDA) levels, indicative of lipid peroxidation, with a 227.18% increase ($n = 4$, $p = 0.04363$) after 2 days and a 188.15% increase ($n = 3$, $p = 0.02778$) after 4 days of treatment. Statistical significance level versus untreated samples: * $p \leq 0.05$, ** $p \leq 0.01$, *** $p \leq 0.001$

Reactive oxygen species

It is well known that A β 42 action is related to increased production of reactive oxygen species (ROS). We thus measured ROS-induced damage by determining levels of key protective enzymes superoxide dismutases (SOD), mainly cytosolic SOD1 and mitochondrial SOD2 (Fig. 5A). Although these enzymes represent the main barrier against oxidative stress connected with ROS, we did not detect any alteration of SOD in any of our experimental settings.

For monitoring ROS-induced damage, we used two independent methods, viz. DCF-DA and TBARS assays. Our results from the DCF-DA assay show significantly increased fluorescence signal only in NaOH-A β 42-treated cells, in both 2- (178% increase) and 4-day (469% increase) exposure, whereas no elevation was observed in the NH₄OH-A β 42 samples (Fig. 5B). This indicates a difference in the action of individual A β 42 species in relation to oxidative stress. We thus wanted to confirm our result by a different method, so we monitored the level of lipid peroxidation, which is a characteristic feature of ROS interaction with membrane lipids. In the TBARS assay, TBA reacts with malondialdehyde (MDA), a cleavage product of lipids produced by ROS in a membrane environment. The reaction product TBARS yields a red–pink color that can be measured spectrophotometrically at 532 nm [85]. As shown in Fig. 5C, we again monitored more than a 150% increase in MDA level, only in NaOH-A β 42-treated cells. We can thus conclude that, in our experiments, only NaOH-A β 42 induced ROS damage, but to an extent that does not activate the anti-ROS protecting system based on SODs.

Effect on mitochondria

As ROS are produced mainly in mitochondria, these organelles are exposed to their action first. Thus, we studied changes in the mitochondrial membrane potential, the level of the main mitochondrial enzyme, the F-ATPase, and the production of mt-TFA (TFAM), all of which may indicate disruption of mitochondrial homeostasis. We measured mitochondrial mass and membrane potential with MitoTracker™ red and MitoTracker™ green, respectively (Fig. 6). Although no alteration in mitochondrial mass was observed, there was a decrease in the mitochondrial membrane potential to 85% in NaOH-A β 42-exposed cells, which was apparent in 4-day A β treatment. This alteration corresponded well to immunoblot analysis of the expression of both F-ATPase and mt-TFA (Fig. 6B). While the amount of F-ATPase significantly decreased in NaOH-A β 42-treated SH-SY5Y cells after 4 days of exposure, to 71.14%, it remained unchanged in NH₄OH-A β 42 application. The reverse was monitored for mt-TFA level, which was increased only in NaOH-A β -treated cells, with a more conspicuous effect after 4 days of amyloid action (~140%). Although the membrane potential was only slightly decreased and no reduction in mitochondrial mass occurred, the decrease of the F-ATPase and elevation of mt-TFA indicates hampering of mitochondrial activity after NaOH-A β 42 action. On the other hand, the NH₄OH-A β 42 seemed not to alter any of the monitored parameters of mitochondrial function.

Calpain activity

In the previous experiments, we observed disruptions of ER and mitochondria, especially in SH-SY5Y cells exposed to NaOH-A β 42. Both these organelles serve as the

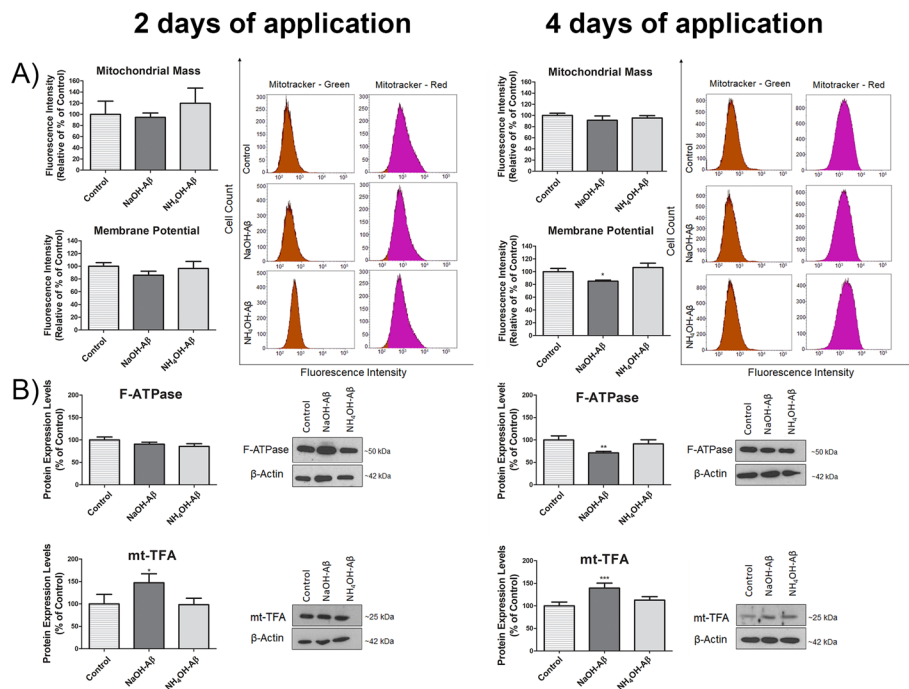


Fig. 6 Analysis of mitochondrial function and protein expression in response to NaOH-Aβ42 and NH₄OH-Aβ42 treatment. **A** MitoTracker analysis showed a decrease in mitochondrial membrane potential in cells exposed to NaOH-Aβ42 after 4 days (85.01%, $n = 3$, $p = 0.02525$), although mitochondrial mass had not changed. **B** The expression levels of F-ATPase showed a significant decrease in NaOH-Aβ42-treated cells after 4 days (71.14%, $n = 3$, $p = 0.00847$), while they remained unchanged when NH₄OH-Aβ42 was applied. Conversely, mt-TFA levels increased only in NaOH-Aβ42 experiments after 2 days (139.18%, $n = 4$, $p = 0.01517$) and 4 days (139.18%, $n = 4$, $p = 0.00054$) of amyloid exposure. Statistical significance level versus untreated samples: * $p \leq 0.05$, ** $p \leq 0.01$, *** $p \leq 0.001$

storage system of intracellular calcium ions. The alterations in ER/mitochondria integrity may thus indicate dyshomeostasis of cytosolic Ca²⁺ concentration. In our study, we concentrated on the long-term effects of Aβ treatment, so we analyzed the activity of Ca²⁺-dependent protease calpain, whose activation is often connected with Aβ action (reviewed in Refs. [1, 111]). Calpain activity is measurable by monitoring the cleavage of spectrin, which serves as a calpain substrate [111, 112]. Our immunoblot analysis showed enhanced spectrin cleavage only in NaOH-Aβ42 4-day experiments, which was measured as a reduction of full-length spectrin (~ 255 kDa) to 65.64% and parallel elevation (120.15%) of lower-kDa spectrin form (~ 150 kDa) (Fig. 7A). We did not analyze other calcium-dependent events as we only wanted to consider the main aspects of the relatively long-term action of different Aβ preparations. In our experiments, we could thus see that calpain, as a marker of elevated cytosolic Ca²⁺ level, was activated only by NaOH-Aβ42 but not by NH₄OH-Aβ42 species.

Heat shock proteins

As we could observe cellular stress on several levels, we may suppose a systemic answer that includes the action of heat shock proteins (Hsp). We analyzed levels

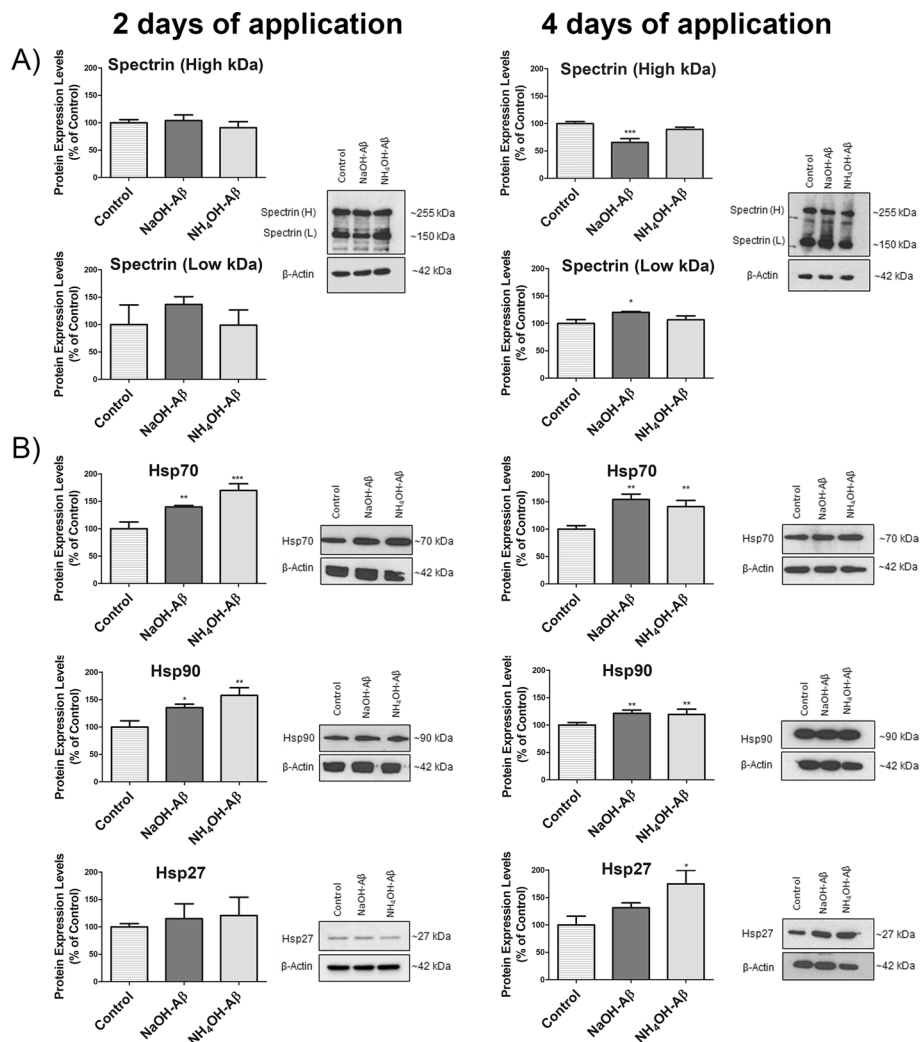


Fig. 7 Analysis of calpain activity and heat shock protein (Hsp) expression in response to NaOH-Aβ₄₂ and NH₄OH-Aβ₄₂ treatment. **A** Enhanced calpain activity was evident only in cells treated with NaOH-Aβ₄₂ for 4 days, as indicated by the reduction of the full-length spectrin form (~255 kDa) to 65.64% ($n=3, p=0.00039$) and parallel elevation of a lower-weight spectrin form (~150 kDa) to 120.15% ($n=3, p=0.01293$). **B** The levels of Hsp70 and Hsp90 showed a consistent increase in response to both NaOH-Aβ₄₂ and NH₄OH-Aβ₄₂ treatments, observed in both 2- and 4-day applications (Hsp70: after 2 days of exposure to NaOH-Aβ₄₂ 139.73%, $n=3, p=0.00735$, and 169.86%, $n=3, p=0.00038$ after NH₄OH-Aβ₄₂ applications, after 4 days of exposure 154.15%, $n=3, p=0.00104$ after NaOH-Aβ₄₂, and 141.05%, $n=3, p=0.00439$ after NH₄OH-Aβ₄₂ application; Hsp90: after 2 days of exposure 135.22%, $n=3, p=0.01930$ after NaOH-Aβ₄₂ and 157.83%, $n=3, p=0.00172$ after NH₄OH-application, after 4 days of exposure 121.41%, $n=3, p=0.00489$ after NaOH-Aβ₄₂ and 119.44%, $n=3, p=0.00877$ after NH₄OH-Aβ₄₂ application). Hsp27, however, was significantly increased only after 4 days of NH₄OH-Aβ₄₂ exposure, indicating a specific protective response (174.89%, $n=3, p=0.00513$). Statistical significance level versus untreated samples: * $p \leq 0.05$, ** $p \leq 0.01$, *** $p \leq 0.001$

of large Hsp (Hsp70 and Hsp90) that serve as molecular chaperons defending cells against misfolded and aggregated proteins [113]. In our experimental system, both Aβ₄₂ preparations caused elevation of large Hsp levels, in all 2- and 4-day

Aβ applications (Fig. 7B). Although we could not see any difference in Hsp70 and Hsp90 content between NaOH-Aβ42- and NH₄OH-Aβ42-treated cells, the reverse was observed for small heat shock protein Hsp27. Here, only after 4-day exposure to NH₄OH-Aβ42, SH-SY5Y cells increased production of this protective protein to 174% (Fig. 7B). This result indicates that both preparations of Aβ activated Hsp associated with response to misfolded/aggregated proteins but only NH₄OH-Aβ42 added also protection that is based on the small Hsp27.

Necroptosis and other cell death pathways

Next, we focused our attention on necroptosis, programmed cell necrosis, which is also associated with AD [46, 114, 115]. In necroptosis, a necrosome complex from RIPK1 and RIPK3 is formed that leads to membrane disruption by MLKL [26, 45–48]. RIPK3 and MLKL as well as their phosphorylated forms may serve as markers of necroptosis [45, 48, 116]. In contrast to ROS-induced damage, we observed elevation of nonphosphorylated

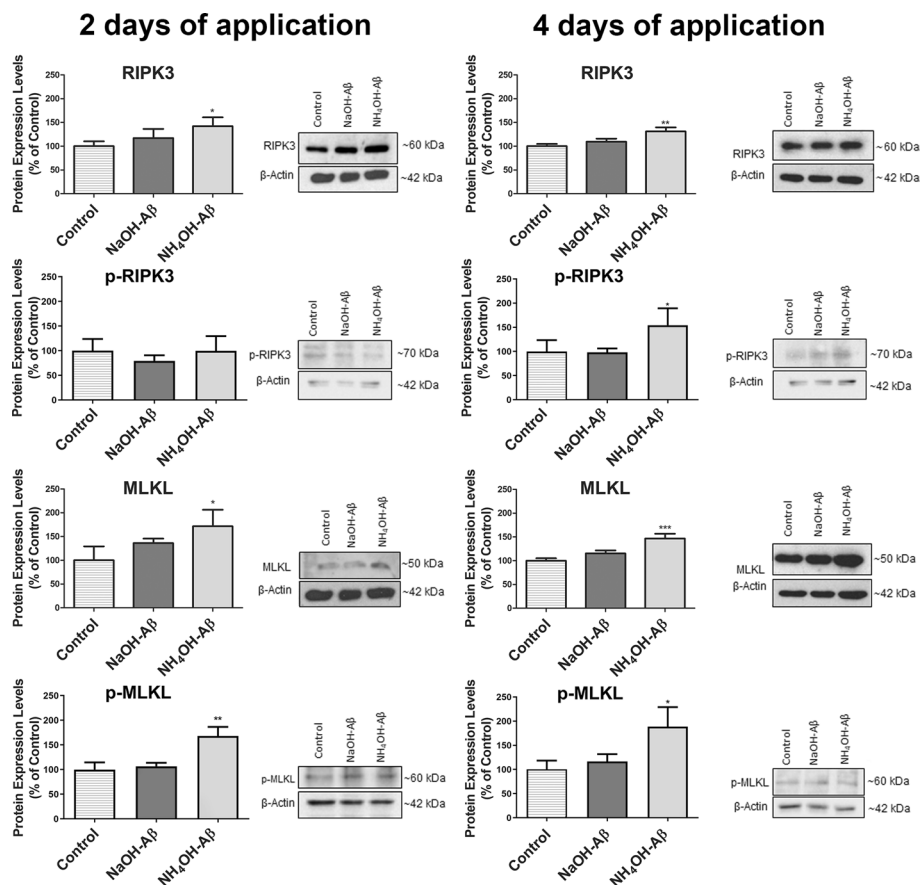


Fig. 8 Quantification of necroptosis markers RIPK3 and MLKL and their phosphorylation in response to NaOH-Aβ42 and NH₄OH-Aβ42 application. Treatment with NH₄OH-Aβ42 for 2 days led to a significant increase in the levels of receptor-interacting protein kinase 3 (RIPK3, 142.23%, *n* = 3, *p* = 0.04589), mixed lineage kinase domain-like pseudokinase (MLKL, 171.49%, *n* = 3, *p* = 0.03958), and phosphorylated-MLKL (168.28%, *n* = 3, *p* = 0.00241). A more pronounced effect was observed after 4 days of NH₄OH-Aβ42 exposure, with a significant increase in RIPK3 (131.18%, *n* = 3, *p* = 0.00319), MLKL (146.77%, *n* = 3, *p* = 0.00513), phosphorylated-RIPK3 (154, 35%, *n* = 4, *p* = 0.03047), and phosphorylated-MLKL (188.54%, *n* = 3, *p* = 0.01676). Statistical significance level versus untreated samples: **p* ≤ 0.05, ***p* ≤ 0.01, ****p* ≤ 0.001

RIPK3 and MLKL only in NH₄OH-Aβ₄₂-exposed SH-SY5Y cells (Fig. 8). There was a clear effect in 2 days of Aβ treatment, but it was more significant in 4-day NH₄OH-Aβ₄₂ exposure. Analysis of RIPK3 and MLKL phosphorylation also indicated more than 170% elevation of these activated participants of necroptosis. On the other hand, no alterations in necroptosis markers were connected to NaOH-Aβ₄₂ action (Fig. 8).

We were also interested in finding out whether other CD pathways might be involved in mediating the effects of Aβ. Measurements of PARP protein levels (a marker of parthanatos) and gasdermin D cleavage (a marker of pyroptosis) did not indicate alterations in these processes. Our results regarding autophagy were controversial, and this topic will be the subject of further research.

Role of GM1

It is possible that NaOH-Aβ₄₂ and NH₄OH-Aβ₄₂ may differ not only in their effect but also in their mechanism of entry into the cell. It is known that Aβ interactions with membrane lipid ganglioside GM1 may affect peptide aggregation, structure, and toxicity (reviewed in Ref. [22]). Using an inhibitor of ganglioside synthesis, D-PDMP [8, 20], we decreased the amount of membrane GM1 to 34.15% via the application

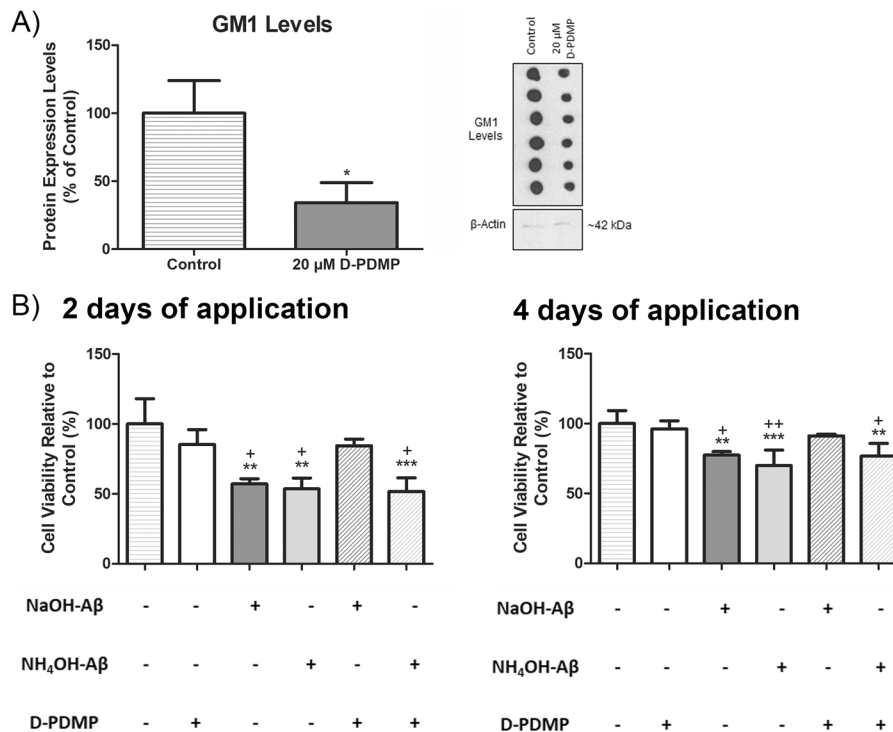


Fig. 9 Modulation of GM1 levels and its impact on cell viability in response to Aβ₄₂ peptides. **A** Treatment with 20 μM D-PDMP for 2 days resulted in a reduction of GM1 to 34.15% ($n = 3, p = 0.0154$); representative dot blot shown on the right. **B** Cells with decreased GM1 levels (D-PDMP+) did not show decreased viability even after 2 and 4 days of NaOH-Aβ₄₂ application. However, cell viability was reduced after NaOH-Aβ₄₂ action with normal GM1 level (D-PDMP-). On the other hand, NH₄OH-Aβ₄₂-treated cells showed unchanged Aβ toxicity even in the presence of D-PDMP (reduced GM1 level) ($n = 3-4$). Statistical significance level versus untreated samples (pluses) or samples treated only with D-PDMP (asterisks): * $^+p \leq 0.05$, ** $^{++}p \leq 0.01$, *** $^{+++}p \leq 0.001$

of 20 μM D-PDMP for 2 days (Fig. 9A). The reduction of GM1 content by D-PDMP was not toxic to the differentiated cells (Supplementary Fig. S2), but it affected the A β action. Under D-PDMP-induced reduction of GM1, the NaOH-A β 42 effect was diminished, and we did not detect any change in cell viability (Fig. 9). However, a similar reduction of GM1 did not affect the A β toxicity of NH₄OH-A β 42, where the viability was decreased to at least 75%, similarly to that with normal GM1 levels (Fig. 9).

Discussion

The main purpose of the present study was to investigate the mechanisms responsible for cell death (CD) mediated by A β 42. Among CD pathways that often may occur simultaneously, apoptosis, necroptosis, pyroptosis, altered autophagy and mitophagy, lysosomal destruction as well as ferroptosis and ROS action or mitochondrial disruption have been described to be associated with AD [16, 30, 32–37, 39–44, 46, 49, 50, 54, 55, 63, 67, 69, 75, 84, 100, 102–105, 114, 115, 117–120]. In our study, we focused on the effect of two distinct A β 42 oligomer species: NaOH-A β 42 and NH₄OH-A β 42. We used differentiated SH-SY5Y neuroblastoma cells that represent a neural-like model suitable for measuring toxicity induced by various substances, including A β 42 [76, 84, 99, 100]. As the time course of A β application may play a role, we compared 2- and 4-day treatments. Although no significant difference in the size of both A β 42 aggregates was found, they differed fundamentally in the type of CD they caused.

We prepared A β oligomers according to the protocols using NaOH or NH₄OH for amyloid solubilization [73–76]. On the basis of DLS and AFM analyses, we do not expect strong differences in size/form and shape of both A β preparations, but it is possible that the size distribution in each population differs slightly. Although some fibrillar forms were observed, most of the particles had circular symmetry and a size corresponding to <20 monomers. On the immunoblot, we could see bands corresponding to A β 42 tetramers and to a much lesser extent also trimers. Antibodies against A β oligomers were not able to recognize these smaller forms, but they distinguished two larger aggregates of ~64 kDa and ~57 kDa MW corresponding to oligomers composed of ~14 and ~12 monomers of A β 42. Whatever the size of the oligomers in our preparations, we could not find any difference in the size and shape of NaOH-A β 42 and NH₄OH-A β 42 aggregates. Thus, owing to their specific effects on cells, we suppose more subtle differences in tertiary or secondary structure. We can only speculate what could be behind this different action of both preparations. We can exclude heterogeneity of A β coming from different sources (we used only one type from Bachem, 107,761–42-2), which may also play a role in the final effect. One potential possibility could be the different chirality of the growing fibrils (initial seeds of fibrils), as revealed by vibrational circular dichroism for mature fibrils [121]. Moreover, the sensitivity of the chiral form to the surrounding environment of growing fibrils, e.g., pH [121, 122], is well documented. Although this appears to be a plausible explanation, it is very difficult to verify in the case of A β (unlike model proteins). It is very hard to characterize relatively small A β initial aggregates more closely owing to the possible emergence of artificial rearrangements during sample manipulations (e.g., concentrations needed for vibrational circular dichroism are extremely high in comparison with those used in our experiments).

Both A β preparations were toxic to differentiated SH-SY5Y cells to a similar extent. We also excluded the toxicity of DMSO and pure NH₄OH (Supplementary Fig. S2), which seems to be highly improbable owing to the very low concentration, high volatility, and long-term incubation. Different concentrations of A β are used experimentally, from <1 μ M to >10 μ M [16, 37, 39, 41, 44, 54, 57, 69, 75, 76, 84, 100, 102, 103, 105, 118, 120]. However, the final effective concentration is hard to establish, as (1) the aggregation process reduces the concentration of A β formations, and (2) cells concentrate A β intracellularly up to >100 μ M [123]. In our experiments, we mainly used the 2.25 μ M starting concentration of A β , but we are aware that, during the aggregation process, the concentration of macromolecular formations decreased ~tenfold compared with the monomers, and that a small amount of A β was lost in the form of larger fibrillar structures during the filtration of A β before addition to the cell culture.

AD is a slow neurodegeneration process, hence longer A β incubation better corresponds to pathophysiological processes in the brain. In almost all our experiments, in comparison with 2-day application, the effects of A β were accentuated after 4 days of exposure, and some of them seemed to just be beginning. Thus, the short incubation times that are widely used [16, 37, 39, 41, 44, 54, 69, 75, 102, 103, 105] may conceal information about processes with slower or delayed progression.

Among the types of CD related to AD, apoptosis may play a significant role [30, 32, 39–41, 44, 75, 100, 102, 103, 105, 119]. We thus focused on determining the contribution of apoptosis to CD caused by our A β 42 preparations. The results from FC and AO/PI assay consistently showed the toxic effect of both NaOH- A β 42 and NH₄OH-A β 42 preparations (Fig. 3), but a weak contribution of apoptosis was observed only in the 4-day NH₄OH-A β exposure. Apoptosis includes a cascade of events where different elements are sequentially activated, including the activation of executioner Cas3. In accordance with the results from FC and AO/PI, we could detect no alteration in both procaspase 3 and the activated (cleaved) form after A β 42 treatment (Fig. 4). Nevertheless, caspase-independent apoptosis was characterized, being associated with the formation of MOMP from BAX or BAK, release of AIF and cytochrome c from mitochondria, and activation of transcription factor p53 [1, 28–32, 124, 125]. In a concentration- and time-dependent way, BAX elevation and antiapoptotic Bcl-XL reduction do not need to induce activation of caspases, but increase cell vulnerability to ROS damage, as was shown on cultivated neurons exposed to A β 42 [28]. Thus, the caspase-independent mechanism of A β toxicity is mediated by BAX-dependent mitochondrial membrane permeabilization and release of ROS [28–30, 32].

In the experiments with NH₄OH-A β 42-treated cells, proapoptotic BAX, BAK, AIF, and p53 increased after 4 days of exposure, indicating apoptosis activation. Although BAX/BAK pore formation may also be started in NaOH-A β 42 preparation, where these proteins were elevated as well, no increase of AIF was observed, implying that full apoptosis was not elicited. However, we monitored only the total amounts of selected markers and not a change in cellular localization that would correspond to the release of AIF from mitochondria into the cytosol. We thus cannot exclude the shifts in cellular localizations that are not connected with alterations in total amounts. However, if they occurred, they were not accompanied by other apoptosis-related events. In accordance with FC and AO/PI, the results from WB analysis indicated that apoptosis

was not a dominant process in A β -induced CD in the SH-SY5Y cell line. However, in NH₄OH-A β 42 action, caspase-independent apoptosis may be involved, as key markers of the initial phase of apoptosis seemed to be activated. The reluctance for apoptosis in our model of differentiated neuroblastoma cells may reflect the fact that mature neurons are resistant to apoptosis more than young cells, as they must survive for tens of years of the organism's life [126].

ER stress represents a mitochondria-independent entry into the apoptosis that is also related to A β -induced damage and is connected with activation of caspases 4/12 and Ca²⁺ release [2, 70, 107, 127, 128]. ATF6 α is a transcription factor that reacts to ER damage and supports apoptosis at multiple levels, including p53 action [124–126, 129]. In our experiments, both preparations of A β 42 induced elevation of ATF6 α as well as Cas12, whose activation was monitored during ER stress in SH-SY5Y cells [109, 110]. Although we did not observe Cas12 cleavage, the elevation of Cas12 and ATF6 α indicates ER stress that may lead to apoptosis [130]. We may thus conclude that ER damage is associated with the action of both NaOH-A β 4 and NH₄OH-A β 42 amyloid preparations.

As A β is known to induce ROS-associated damage [34, 39–44, 105], levels of superoxide dismutase (SOD) may mirror activation of anti-ROS defense. SOD2 was found to be protective against A β action [131], but A β induced a decrease of SOD2 in mouse and human AD brains [132, 133]. A β was also shown to reduce the activity of SOD1 [134] and the brain level of SOD1 decreased in AD human subjects [135], which may correspond to increased ROS-induced stress [136]. On the other hand, A β oligomers stimulated SOD1 activity in cultured neurons and in human AD brain [137]. Hence, SOD upregulation may compensate for ROS-induced damage [136]. The controversy regarding SOD1/2 alterations in AD reflects insufficient data, the use of different brain tissues, and the influences of other factors, including tau pathology as well as the time course. Both SODs were reduced at 3 and 18 months but increased in the 12-month-old brain neocortex of mice model of AD, which may indicate a loss of antioxidant capacity in the later stadia of AD [138]. However, no alterations in the amounts of SODs were monitored in our experiments.

Although the protective action of SODs was not activated in our system, ROS production was enhanced. Production of intracellular ROS can be detected by the DCF-DA assay, where dichlorofluorescein (DCF) gives a fluorescence signal after ROS-mediated oxidation [42]. In the TBARS assay, the level of malondialdehyde (MDA) is measured by a reaction where the product TBARS may be evaluated spectrophotometrically [86]. Our results from both measurements clearly showed increased ROS production only in NaOH-A β 42, and not in NH₄OH-A β 42-treated SH-SY5Y cells. The effect was observed in both 2- and 4-day experiments, which means a stable and relatively long-term oxidative stress. Higher ROS damage in NaOH-A β 42-treated cells was surprising as ROS-induced deleterious processes are interconnected with apoptosis and our measurements of apoptosis indicated a stronger effect in NH₄OH-A β 42-exposed SH-SY5Y cells.

AD-related mitochondrial dysfunction induced by A β is associated with alterations in the mitochondrial membrane potential [6, 43, 69, 84, 120, 139]. Our data confirmed this effect, but only in the case of NaOH-A β 42 action. Although no reduction in

mitochondrial mass was observed, the key enzyme, F-ATPase (ATP-synthase) amount was lowered in NaOH-A β 42-treated SH-SY5Y cells. F-ATPase was shown to be decreased in AD brains [140], and it serves as a substratum of ROS in AD [113, 141]. Our observation of decreased F-ATPase amount in NaOH-A β 42-exposed cells corresponds to the elevation of oxidative stress measured by DCF-DA and TBARS assays.

Mt-TFA (TFAM) participates in the regulation of Ca²⁺ and ROS levels as it is a part of a protective system for mitochondrial DNA [105, 142–144]. Mitochondrial ROS may suppress mt-TFA expression [144, 145], and a decreased amount of mt-TFA was observed in human AD hippocampi and the M17 cellular model of AD [146]. On the other hand, mt-TFA elevation may serve as a compensation mechanism even toward A β 42-induced ROS damage [142, 147]. The overexpression of mt-TFA attenuated A β -induced oxidative damage of mitochondrial DNA in SH-SY5Y cells [105]. In our experiments, mt-TFA was elevated only in NaOH-A β 42-exposed cells, especially after 4 days of treatment. This indicates activation of anti-ROS defense at the level of mitochondria, although we did not monitor any effect on mitochondrial SOD2 level. Based on obtained data, we can conclude that NaOH-A β 42, but not NH₄OH-A β 42, is connected with ROS-induced damage of mitochondrial function and at least partial activation of protective processes represented by elevation of mt-TFA.

Amyloid β may cause calcium dyshomeostasis by enhancing the Ca²⁺ permeability of plasma, ER, or mitochondrial membrane [1, 3, 6, 16, 43, 148, 149]. In AD, elevated intracellular Ca²⁺ level activates calpain protease, which may lead to CD [1, 111, 112]. Because we observed disruption of both main Ca²⁺ storage systems, ER and mitochondria, which was accentuated in NaOH-A β 42 exposure, Ca²⁺ dyshomeostasis seemed highly probable. We thus analyzed calpain activity by measuring the cleavage of calpain substrate, spectrin [111, 112]. As the main aim of our study was a characterization of the long-term effects of A β 42, calpain activation represented a system responding to prolonged A β treatment and our results showed that only in 4-day treatment with NaOH-A β 42 preparation was spectrin cleavage increased. This indicates that Ca²⁺-dependent processes including calpain activation are associated with longer times of A β exposure, as we did not observe enhanced spectrin cleavage in 2-day experiments. We recorded ER stress (ATF6 α and Cas12 elevations) in both A β preparations, but calpain activation and mitochondrial damage were apparent only in NaOH-A β 42 exposures, and not in NH₄OH-A β 42 treatment. Thus, we can hypothesize that Ca²⁺ ions were released from mitochondria and not from ER, as only 4 days of NaOH-A β 42 exposure led to calpain activation.

Among protective mechanisms activated by A β , Hsp may play a role. Small Hsp, including Hsp27 (HspB1), may protect cells against ROS and thus be elevated in AD. Hsp27 was shown to act antiapoptotically at several levels, mainly by interacting with BAK, BAX, p53, cytochrome c, PI3K/Akt, or caspases (reviewed in Ref. [108]), but also by reducing A β toxicity by affecting its quaternary structure [150, 151]. On the other hand, the large neuroprotective Hsp (including Hsp70) were lowered in AD brains (reviewed in Ref. [151]). However, in our experiments, the levels of Hsp70 and Hsp90 were increased, which may mean activation of protective system related to misfolded and aggregated proteins [113, 151–153]. Our data thus show that, although both A β preparations, NaOH-A β 42 and NH₄OH-A β 42, activated protection against elevated misfolded/

aggregated proteins based on Hsp70 and Hsp90, only in the case of $\text{NH}_4\text{OH-A}\beta 42$ exposures was antiapoptotic and anti-ROS protection mediated by Hsp27 also initiated.

Among other AD-associated CD mechanisms, necroptosis may play a role in neurodegeneration [46, 114, 115]. Necroptosis is initiated mainly when the activity of caspases is reduced, e.g., in mature neurons [126], where necroptosis may be the main actor in regulated CD [48]. Necroptosis is associated with creation of a multiprotein complex (necrosome) from receptor-interacting protein kinases (RIPK) 1 and 3, whose cooperation leads to phosphorylation and oligomerization of mixed lineage kinase domain-like pseudokinase (MLKL), bilayer permeabilization, and CD [26, 45–48]. Elevated and phosphorylated RIPK1 and MLKL were monitored in AD [36]. Necroptosis activation was observed also in neurons of human AD brains in relation to tau pathology or after tumor necrosis factor (TNF)- α secretion by microglia [46, 154, 155]. In a recent study, $\text{A}\beta$ induced necroptosis even in the SH-SY5Y cell model [114].

In our experiments, only $\text{NH}_4\text{OH-A}\beta 42$ induced activation of necroptosis, which was measured as an increased amount and phosphorylation of both RIPK3 and MLKL. This result is somewhat surprising. On the basis of previous measurements, we supposed a necrotic process, but the activation of necroptosis in $\text{NH}_4\text{OH-A}\beta 42$ -treated cells was not as expected. This is because necroptosis and apoptosis may behave as mutually competitive, especially owing to the distinct and mutually exclusive roles of RIPK1 in both processes [25, 26, 48, 65]. We can speculate that necroptosis is more likely to be activated in the earlier stages, while the apoptosis begins to emerge later, as we observed some apoptotic signals mainly after 4-day exposure to $\text{NH}_4\text{OH-A}\beta 42$ but still without activation of caspases. It would be very interesting to look at an even longer time scales of $\text{A}\beta$ action.

Besides the time-course dependence, spatially directed response may also play a role. Different pathways may be activated in different cells, or even within different cell compartments. This was shown in the case of glutamate-mediated excitotoxicity, which was associated with apoptotic events in neuronal soma but with necroptosis in axons [156, 157]. We may thus hypothesize that the variability of the response to $\text{A}\beta$ is connected to different intracellular contexts, the characteristics of particular $\text{A}\beta$ forms, the time scale of $\text{A}\beta$ action, and the membrane properties of a responsive cell.

It is well known that $\text{A}\beta$ interacts with membrane receptors, including proteins and lipids. Among them, ganglioside GM1 was described as one of the most important $\text{A}\beta$ partners [8, 20, 22, 158–163]. We thus compared the effects of $\text{NaOH-A}\beta 42$ and $\text{NH}_4\text{OH-A}\beta 42$ on differentiated SH-SY5Y cell viability after decreasing the GM1 level with D-PDMP, the inhibitor of GM1 synthesis [20, 164]. In our experiments, D-PDMP was not toxic to cells and reduced GM1 levels effectively. What was interesting was the observation that reducing the GM1 level decreased the toxicity only of the $\text{NaOH-A}\beta 42$ preparation, while the toxicity of $\text{NH}_4\text{OH-A}\beta 42$ remained unchanged. This indicates that $\text{NaOH-A}\beta 42$ needs interaction with GM1 to mediate CD, while the toxicity of $\text{NH}_4\text{OH-A}\beta 42$ is GM1 independent. This result is especially interesting as various experimental groups have found distinct involvement of GM1, cholesterol, or sphingomyelin in $\text{A}\beta$ -induced toxicity [17, 22, 23, 161, 165–167]. On the basis of observation, a part of this variability may be associated with distinct characteristics of particular $\text{A}\beta$ species.

Finally, we also attempted to characterize other CD systems, including pyroptosis and autophagy, which are known to play a role in AD [26, 49, 50, 53–57, 63, 67, 117]. We

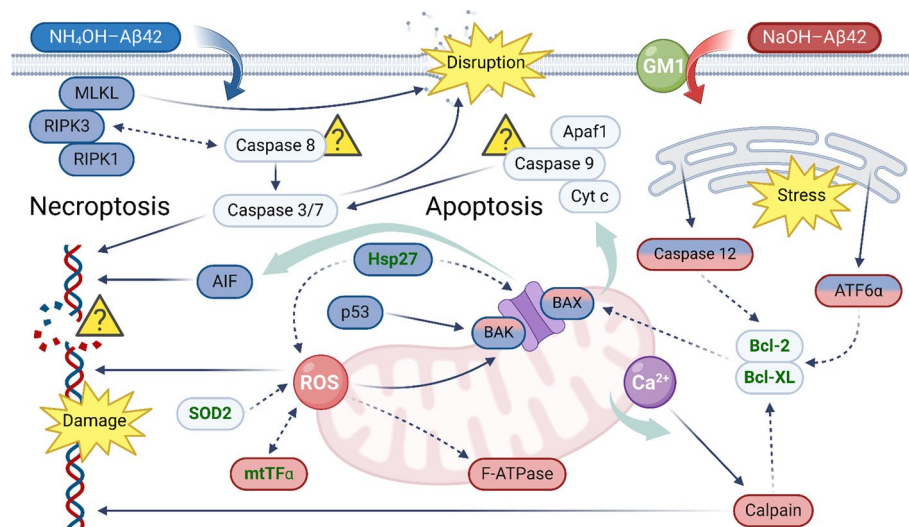


Fig. 10 Diagram summarizing the presumed effect of the two Aβ42 preparations. NaOH-Aβ42 (red) mainly causes impairment of mitochondrial functions (increase of mt-Tfα, decrease in F-ATPase, reduction in membrane potential) and induces damage by reactive oxygen species (ROS). At the same time, it activates calpain, which is related to the dysregulation of Ca²⁺ concentration. The toxicity of NaOH-Aβ42 depends on the amount of ganglioside GM1 in the membrane. In contrast, NH₄OH-Aβ42 (blue) does not require GM1 and its action involves caspase-independent apoptosis-associated events and activation of necroptosis. In parallel, Hsp27-based protection against ROS is also activated. The amplification of endoplasmic reticulum stress appears to be common to both pathways, as well as an increase in BAX/BAK levels, indicating the formation of mitochondrial outer membrane pore. Prosurvival proteins are marked in green, and cell death-supporting elements in black. The solid arrows indicate positive effects, the dashed arrows show inhibitory effects, and the bold blue arrows indicate movement between compartments. We did not analyze DNA damage or shifts and levels of proapoptotic elements (caspase 8, 9, Apaf1 and cytochrome c, indicated by a question mark) as we assume that only initial steps of apoptosis take place. AIF, apoptosis-inducing factor; Cyt c, cytochrome c; MLKL, mixed lineage kinase domain-like pseudokinase; RIPK, receptor-interacting protein kinase; SOD, superoxide dismutase. (Created with BioRender.com)

did not record any alterations in levels and cleavage of PARP1 (marker of parthanatos) and gasdermin D (a marker of pyroptosis) (Supplementary Fig. 4). On the contrary, our results on autophagy remain ambiguous (not shown), and we will address the Aβ-induced alterations in autophagy in later studies.

Conclusions

Taken together, our observations show marked differences in the effects of two preparations of Aβ42, even though we could not see any distinction in their size and shape. Figure 10 indicates possible CD pathways initiated by NaOH-Aβ42 and NH₄OH-Aβ42. The NaOH-Aβ42 preparation is connected to enhanced ROS production and associated disruption of mitochondrial integrity and function. On the other hand, the NH₄OH-Aβ42 preparation is associated more with necroptosis and initiation of apoptosis, while mitochondria remain intact. Both amyloid species induce the first steps of apoptosis, and ER stress, and elevate Hsp-dependent protection against misfolded proteins. Only in NH₄OH-Aβ42 action is the anti-ROS Hsp27 also elevated. We do not know whether the increased amount of Hsp27 or inability of this specific Aβ species to induce ROS-associated stress is responsible for the differences in mitochondrial damage of both preparations. As our measurements clearly showed necrosis to be present,

the PM disruption occurred in all instances. Moreover, GM1 seems to play a distinct role in mechanisms of NaOH-A β 42 and NH₄OH-A β 42 entry into the cell.

Our study has several limitations. First, we were not able to more closely characterize the structural differences between the two amyloid preparations. Second, we only outlined possible CD pathways activated by NaOH-A β 42 and NH₄OH-A β 42, and we omitted many aspects of CD pathways. Third, the SH-SY5Y model is a very specific cellular system that in many ways does not correspond to brain neurons. In the future, we would like to further characterize the molecular structure of both A β preparations, to specify and extend the spectrum of analyzed intracellular processes associated with A β action, and finally to use another cellular model, preferably neural stem cells. It must be stressed here that different models inherently provide different data as A β -induced toxicity seems to be extremely sensitive to the context of its action, including membrane characteristics as well as the specific cytosolic environment. Thus, if even relatively small differences in the structure of a toxic amyloid preparation can play a role in its mechanism of action, it is not surprising that dozens or hundreds of studies have reached different results. It follows that all aspects related to the preparation of the AD model must be given the utmost attention. On the other hand, the different data from the brains of AD patients show that, even in vivo, not only is there variability in the toxic forms of A β but that the variability of the described damage fully corresponds to the diversity of tissues and cell types.

Abbreviations

A β 42	Amyloid β 42
AD	Alzheimer's disease
AIF	Apoptosis inducing factor
AO	Acridine Orange
Cas	Caspase
CD	Cell death
DCF-DA	2',7'-Dichlorodihydrofluorescein diacetate
DLS	Dynamic light scattering
DMSO	Dimethyl sulfoxide
D-PDMP	<i>N</i> -[(1 <i>R</i> ,2)-2-hydroxy-1-(4-morpholinylmethyl)-2-phenylethyl]-decanamide
ER	Endoplasmic reticulum
FC	Flow cytometry
GM1	Monosialotetrahexosylganglioside
HFIP	1,1,1,3,3,3-Hexafluoro-2-propanol
Hsp	Heat shock proteins
MDA	Malondialdehyde
MLKL	Mixed lineage kinase domain-like pseudokinase
MOMP	Mitochondrial outer membrane pore
MTT	3-(4,5-Dimethylthiazol-2-yl)-2,5-diphenyltetrazolium bromide
mt-TFA (TFAM)	Mitochondrial transcription factor A
MW	Molecular weight
PI	Propidium iodide
PM	Plasma membrane
RIPK	Receptor-interacting protein kinase
ROS	Reactive oxygen species
SOD	Superoxide dismutase
TBA	Thiobarbituric acid
TBARS	Thiobarbituric acid reactive substances
TCA	Trichloroacetic acid
WB	Western blot

Supplementary Information

The online version contains supplementary material available at <https://doi.org/10.1186/s11658-024-00657-8>.

Additional file 1.

Acknowledgements

Not applicable.

Author contributions

A.Y.Ö. performed the vast majority of experiments and statistical evaluation of the data. K.H. performed DLS and AFM measurements and participated in data processing. V.K. assisted with interpretation of DLS and AFM results and editing of the manuscript. J.N. helped with editing the text and planning the experiments. V.R. planned most of the experiments and was a major contributor in data interpretation and writing the manuscript. All authors read and approved the final manuscript.

Funding

This work was supported by Charles University Institutional Project SVV-260683.

Availability of data and materials

The data generated or analyzed during this study are included in this published article and its supplementary information files. All original WB and other direct outputs from measurements can be sent by the authors upon request.

Declarations**Ethics approval and consent to participate**

Not applicable.

Consent for publication

Not applicable.

Competing interests

The authors declare that they have no competing interests.

Received: 19 July 2024 Accepted: 22 October 2024

Published online: 17 November 2024

References

1. Fricker M, Tolkovsky AM, Borutaite V, Coleman M, Brown GC. Neuronal cell death. *Physiol Rev*. 2018;98:813–80.
2. Chafekar SM, Hoozemans JJ, Zwart R, Baas F, Scheper W. Aβ_{1–42} induces mild endoplasmic reticulum stress in an aggregation state-dependent manner. *Antioxid Redox Signal*. 2007;9:2245–54.
3. Resende R, Ferreira E, Pereira C, De Oliveira CR. Neurotoxic effect of oligomeric and fibrillar species of amyloid-beta peptide 1–42: Involvement of endoplasmic reticulum calcium release in oligomer-induced cell death. *Neuroscience*. 2008;155:725–37.
4. Picone P, Carrotta R, Montana G, Nobile MR, Biagio PLS, Di Carlo M. Aβ oligomers and fibrillar aggregates induce different apoptotic pathways in LAN5 neuroblastoma cell cultures. *Biophys J*. 2009;96:4200–11.
5. Bucciantini M, Rigacci S, Stefani M. Amyloid aggregation: role of biological membranes and the aggregate-membrane system. *J Phys Chem Lett*. 2014;5:517–27.
6. Jekabsons A, Jankeviciute S, Pampuscenko K, Borutaite V, Morkuniene R. The role of intracellular Ca and mitochondrial ROS in small Aβ oligomer-induced microglial death. *Int J Mol Sci*. 2023;24:12315.
7. Lambert MP, Barlow AK, Chromy BA, Edwards C, Freed R, Liosatos M, et al. Diffusible, nonfibrillar ligands derived from Aβ are potent central nervous system neurotoxins. *Proc Natl Acad Sci USA*. 1998;95:6448–53.
8. Yamamoto N, Matsubara E, Maeda S, Minagawa H, Takashima A, Maruyama W, et al. A ganglioside-induced toxic soluble Aβ assembly -: its enhanced formation from Aβ bearing the arctic mutation. *J Biol Chem*. 2007;282:2646–55.
9. Bernstein SL, Dupuis NF, Lazo ND, Wytenbach T, Condron MM, Bitan G, et al. Amyloid-β protein oligomerization and the importance of tetramers and dodecamers in the aetiology of Alzheimer's disease. *Nat Chem*. 2009;1:326–31.
10. Williams TL, Johnson BR, Urbanc B, Jenkins AT, Connell SD, Serpell LC. Aβ₄₂ oligomers, but not fibrils, simultaneously bind to and cause damage to ganglioside-containing lipid membranes. *Biochem J*. 2011;439:67–77.
11. Cline EN, Bicca MA, Viola KL, Klein WL. The amyloid-β oligomer hypothesis: beginning of the third decade. *J Alzheimers Dis*. 2018;64:S567–610.
12. Ewald M, Henry S, Lambert E, Feuillie C, Bobo C, Cullin C, et al. High speed atomic force microscopy to investigate the interactions between toxic A peptides and model membranes in real time: impact of the membrane composition. *Nanoscale*. 2019;11:7229–38.
13. Xue C, Tran J, Wang HS, Park G, Hsu F, Guo ZF. Aβ₄₂ fibril formation from predominantly oligomeric samples suggests a link between oligomer heterogeneity and fibril polymorphism. *R Soc Open Sci*. 2019;6: 190179.
14. Cizas P, Budytyte R, Morkuniene R, Moldovan R, Broccio M, Lösche M, et al. Size-dependent neurotoxicity of β-amyloid oligomers. *Arch Biochem Biophys*. 2010;496:84–92.
15. Hartley DM, Walsh DM, Ye CPP, Diehl T, Vasquez S, Vassilev PM, et al. Protofibrillar intermediates of amyloid β-protein induce acute electrophysiological changes and progressive neurotoxicity in cortical neurons. *J Neurosci*. 1999;19:8876–84.

16. Takada E, Okubo K, Yano Y, Iida K, Someda M, Hirasawa A, et al. Molecular mechanism of apoptosis by amyloid β -Protein fibrils formed on neuronal cells. *ACS Chem Neurosci*. 2020;11:796–805.
17. Yuyama K, Yanagisawa K. Sphingomyelin accumulation provides a favorable milieu for GM1 ganglioside-induced assembly of amyloid beta-protein. *Neurosci Lett*. 2010;481:168–72.
18. Viola KL, Klein WL. Amyloid β oligomers in Alzheimer's disease pathogenesis, treatment, and diagnosis. *Acta Neuropathol*. 2015;129:183–206.
19. Evangelisti E, Cascella R, Becatti M, Marrazza G, Dobson CM, Chiti F, et al. Binding affinity of amyloid oligomers to cellular membranes is a generic indicator of cellular dysfunction in protein misfolding diseases. *Sci Rep UK*. 2016;6:32721.
20. Fernández-Pérez EJ, Sepúlveda FJ, Peoples R, Aguayo LG. Role of membrane GM1 on early neuronal membrane actions of A β during onset of Alzheimer's disease. *BBA Mol Basis Dis*. 2017;1863:3105–16.
21. Chen GF, Xu TH, Yan Y, Zhou YR, Jiang Y, Melcher K, et al. Amyloid beta: structure, biology and structure-based therapeutic development. *Acta Pharmacol Sin*. 2017;38:1205–35.
22. Rudajev V, Novotny J. The role of lipid environment in ganglioside GM1-induced amyloid β aggregation. *Membranes-Basel*. 2020;10:226.
23. Rudajev V, Novotny J. Cholesterol as a key player in amyloid β -mediated toxicity in Alzheimer's disease. *Front Mol Neurosci*. 2022;15: 937056.
24. Orrenius S, Gogvadze A, Zhivotovsky B. Mitochondrial oxidative stress: Implications for cell death. *Annu Rev Pharmacol*. 2007;7:143–83.
25. Vanden Berghe T, Kaiser WJ, Bertrand MJM, Vandenabeele P. Molecular crosstalk between apoptosis, necroptosis, and survival signaling. *Mol Cell Oncol*. 2015;2: e975093.
26. Choi SB, Kwon S, Kim JH, Ahn NH, Lee JH, Yang SH. The molecular mechanisms of neuroinflammation in Alzheimer's disease, the consequence of neural cell death. *Int J Mol Sci*. 2023;24:11757.
27. Wu HJ, Che XR, Zheng QL, Wu A, Pan K, Shao AW, et al. Caspases: a molecular switch node in the crosstalk between autophagy and apoptosis. *Int J Biol Sci*. 2014;10:1072–83.
28. Paradis E, Douillard H, Koutroumanis M, Goodyer C, LeBlanc A. Amyloid beta peptide of Alzheimer's disease down-regulates bcl-2 and upregulates bax expression in human neurons. *J Neurosci*. 1996;16:7533–9.
29. Su JH, Deng GM, Cotman CW. Bax protein expression is increased in Alzheimer's brain: Correlations with DNA damage, Bcl-2 expression, and brain pathology. *J Neuropath Exp Neur*. 1997;56:86–93.
30. Selznick LA, Zheng TS, Flavell RA, Rakic P, Roth KA. Amyloid beta-induced neuronal death is bax-dependent but caspase-independent. *J Neuropath Exp Neur*. 2000;59:271–9.
31. Dewson G, Kluck RM. Mechanisms by which Bak and Bax permeabilise mitochondria during apoptosis. *J Cell Sci*. 2009;122:2801–8.
32. Kudo W, Lee HP, Smith MA, Zhu X, Matsuyama S, Lee HG. Inhibition of Bax protects neuronal cells from oligomeric A β neurotoxicity. *Cell Death Dis*. 2012;3: e309.
33. Zhao Y, Zhao BL. Oxidative stress and the pathogenesis of Alzheimer's disease. *Oxid Med Cell Longev*. 2013;2013: 316523.
34. Cheignon C, Tomas M, Bonnefont-Rousselot D, Faller P, Hureau C, Collin F. Oxidative stress and the amyloid beta peptide in Alzheimer's disease. *Redox Biol*. 2018;14:450–64.
35. Peña-Bautista C, Vigor C, Galano JM, Oger C, Durand T, Ferrer I, et al. Plasma lipid peroxidation biomarkers for early and non-invasive Alzheimer disease detection. *Free Radical Bio Med*. 2018;124:388–94.
36. Park MW, Cha HW, Kim J, Kim JH, Yang H, Yoon S, et al. NOX4 promotes ferroptosis of astrocytes by oxidative stress-induced lipid peroxidation via the impairment of mitochondrial metabolism in Alzheimer's diseases. *Redox Biol*. 2021;41: 101947.
37. Baruah P, Moorthy H, Ramesh M, Padhi D, Govindaraju T. A natural polyphenol activates and enhances GPX4 to mitigate amyloid- β induced ferroptosis in Alzheimer's disease. *Chem Sci*. 2023;14:9427–38.
38. Zhao D, Yang KL, Guo H, Zeng JS, Wang SS, Xu H, et al. Mechanisms of ferroptosis in Alzheimer's disease and therapeutic effects of natural plant products: a review. *Biomed Pharmacother*. 2023;164: 114312.
39. Zhang JJ, Zhang RF, Meng XK. Protective effect of pyrroloquinoline quinone against A β -induced neurotoxicity in human neuroblastoma SH-SY5Y cells. *Neurosci Lett*. 2009;464:165–9.
40. Ding HT, Wang HT, Zhao YX, Sun DK, Zhai X. Protective effects of baicalin on A β -induced learning and memory deficit, oxidative stress, and apoptosis in rat. *Cell Mol Neurobiol*. 2015;35:623–32.
41. Oguchi T, Ono R, Tsuji M, Shozawa H, Somei M, Inagaki M, et al. Cilostazol suppresses A β -induced Neurotoxicity in SH-SY5Y cells through inhibition of oxidative stress and MAPK signaling pathway. *Front Aging Neurosci*. 2017;9:337.
42. Butterfield DA, Boyd-Kimball D. Oxidative stress, amyloid- β peptide, and altered key molecular pathways in the pathogenesis and progression of Alzheimer's disease. *J Alzheimers Dis*. 2018;62:1345–67.
43. Cinar R, Naziroglu M. TRPM2 channel inhibition attenuates amyloid β 42-induced apoptosis and oxidative stress in the hippocampus of mice. *Cell Mol Neurobiol*. 2023;43:1335–53.
44. Zhang GH, Chin KL, Yan SY, Pare R. Antioxidant and antiapoptotic effects of thymosin β 4 in A β -induced SH-SY5Y cells via the 5-HTR1A/ERK axis. *PLoS ONE*. 2023;18: e0287817.
45. Chen X, Li W, Ren J, Huang D, He WT, Song Y, et al. Translocation of mixed lineage kinase domain-like protein to plasma membrane leads to necrotic cell death. *Cell Res*. 2014;24:105–21.
46. Caccamo A, Branca C, Piras IS, Ferreira E, Huentelman MJ, Liang WS, et al. Necroptosis activation in Alzheimer's disease. *Nat Neurosci*. 2017;20:1236–46.
47. Mompeán M, Li WB, Li JX, Laage S, Siemer AB, Bozkurt G, et al. The structure of the necrosome RIPK1-RIPK3, a human hetero-amyloid signaling complex. *Cell*. 2018;173:1244–53.
48. Li S, Qu LL, Wang XB, Kong LY. Novel insights into RIPK1 as a promising target for future Alzheimer's disease treatment. *Pharmacol Therapeut*. 2022;231: 107979.
49. Bai YL, Liu D, Zhang HH, Wang YY, Wang DG, Cai HB, et al. N-salicyloyl tryptamine derivatives as potential therapeutic agents for Alzheimer's disease with neuroprotective effects. *Bioorg Chem*. 2021;115: 105255.

50. Huang YH, Li XY, Luo GF, Wang JL, Li RH, Zhou CY, et al. Pyroptosis as a candidate therapeutic target for Alzheimer's disease. *Front Aging Neurosci.* 2022;14: 996646.
51. Lee JH, Yang DS, Goulbourne CN, Im E, Stavrides P, Pensalfini A, et al. Faulty autolysosome acidification in Alzheimer's disease mouse models induces autophagic build-up of A β in neurons, yielding senile plaques. *Nat Neurosci.* 2022;25:688–701.
52. Zaretsky DV, Zaretskaia MV, Molkov YI. Membrane channel hypothesis of lysosomal permeabilization by beta-amyloid. *Neurosci Lett.* 2022;770: 136338.
53. Lipinski MM, Zheng B, Lu T, Yan ZY, Py BF, Ng A, et al. Genome-wide analysis reveals mechanisms modulating autophagy in normal brain aging and in Alzheimer's disease. *Proc Natl Acad Sci USA.* 2010;107:14164–9.
54. Wang HM, Ma JF, Tan YY, Wang ZQ, Sheng CY, Chen SD, et al. Amyloid- β induces reactive oxygen species-mediated autophagic cell death in U87 and SH-SY5Y Cells. *J Alzheimers Dis.* 2010;21:597–610.
55. Saleem S, Biswas SC. Tribbles pseudokinase 3 induces both apoptosis and autophagy in amyloid-beta-induced neuronal death. *J Biol Chem.* 2017;292:2571–85.
56. Fang EF, Hou YJ, Palikaras K, Adriaanse BA, Kerr JS, Yang BM, et al. Mitophagy inhibits amyloid- β and tau pathology and reverses cognitive deficits in models of Alzheimer's disease. *Nat Neurosci.* 2019;22:401–12.
57. Wang W, Gu X, Cheng Z, Lu X, Xie S, Liu X. IKKbeta alleviates neuron injury in Alzheimer's disease via regulating autophagy and RIPK1-mediated necroptosis. *Mol Neurobiol.* 2022;59:2407–23.
58. Bassik MC, Scorran L, Oakes SA, Pozzan T, Korsmeyer SJ. Phosphorylation of BCL-2 regulates ER Ca homeostasis and apoptosis. *EMBO J.* 2004;23:1207–16.
59. Wei Y, Sinha S, Levine B. Dual role of JNK1-mediated phosphorylation of Bcl-2 in autophagy and apoptosis regulation. *Autophagy.* 2008;4:949–51.
60. Wirawan E, Vande Walle L, Kersse K, Cornelis S, Claeys H, Vanoverbergh I, et al. Caspase-mediated cleavage of Beclin-1 inactivates Beclin-1-induced autophagy and enhances apoptosis by promoting the release of proapoptotic factors from mitochondria. *Cell Death Dis.* 2010;1: e18.
61. Rubinstein AD, Kimchi A. Life in the balance - a mechanistic view of the crosstalk between autophagy and apoptosis. *J Cell Sci.* 2012;125:5259–68.
62. Charan RA, Johnson BN, Zaganelli S, Nardozi JD, LaVoie MJ. Inhibition of apoptotic Bax translocation to the mitochondria is a central function of parkin. *Cell Death Dis.* 2014;5: e1313.
63. Saleem S. Apoptosis, autophagy, necrosis and their multi galore crosstalk in neurodegeneration. *Neuroscience.* 2021;469:162–74.
64. Gurung P, Anand PK, Malireddi RKS, Walle LV, Van Opendenbosch N, Dillon CP, et al. FADD and caspase-8 mediate priming and activation of the canonical and noncanonical Nlrp3 inflammasomes. *J Immunol.* 2014;192:1835–46.
65. Orozco S, Yatim N, Werner MR, Tran H, Gunja SY, Tait SWG, et al. RIPK1 both positively and negatively regulates RIPK3 oligomerization and necroptosis. *Cell Death Differ.* 2014;21:1511–21.
66. Henry CM, Martin SJ. Caspase-8 acts in a non-enzymatic role as a scaffold for assembly of a pro-inflammatory "FADDosome" complex upon TRAIL stimulation. *Mol Cell.* 2017;65:715–29.
67. Kumar S, Budhathoki S, Oliveira CB, Kahle AD, Calhan OY, Lukens JR, et al. Role of the caspase-8/RIPK3 axis in Alzheimer's disease pathogenesis and A β -induced NLRP3 inflammasome activation. *JCI Insight.* 2023;8: e157433.
68. Demuro A, Mina E, Kayed R, Milton SC, Parker I, Glabe CG. Calcium dysregulation and membrane disruption as a ubiquitous neurotoxic mechanism of soluble amyloid oligomers. *J Biol Chem.* 2005;280:17294–300.
69. Calvo-Rodriguez M, Hernando-Perez E, Nuñez L, Villalobos C. Amyloid β oligomers increase ER-mitochondria crosstalk in young hippocampal neurons and exacerbate aging-induced intracellular Ca remodeling. *Front Cell Neurosci.* 2019;13:22.
70. Maiuri MC, Zalckvar E, Kimchi A, Kroemer G. Self-eating and self-killing: crosstalk between autophagy and apoptosis. *Nat Rev Mol Cell Bio.* 2007;8:741–52.
71. Ku B, Woo JS, Liang C, Lee KH, Jung JU, Oh BH. An insight into the mechanistic role of Beclin 1 and its inhibition by pro-survival Bcl-2 family proteins. *Autophagy.* 2008;4:519–20.
72. Naderi S, Khodaghali F, Pourbadie HG, Naderi N, Rafei S, Janahmadi M, et al. Role of amyloid beta (25–35) neurotoxicity in the ferroptosis and necroptosis as modalities of regulated cell death in Alzheimer's disease. *Neurotoxicology.* 2023;94:71–86.
73. Ciccotosto GD, Tew DJ, Drew SC, Smith DG, Johanssen T, Lal V, et al. Stereospecific interactions are necessary for Alzheimer disease amyloid- β toxicity. *Neurobiol Aging.* 2011;32:235–48.
74. Ryan TM, Caine J, Mertens HDT, Kirby N, Nigro J, Breheny K, et al. Ammonium hydroxide treatment of A β produces an aggregate free solution suitable for biophysical and cell culture characterization. *PeerJ.* 2013;1: e73.
75. Geng LJ, Liu W, Chen Y. Tanshinone IIA attenuates A β -induced neurotoxicity by down-regulating COX-2 expression and PGE2 synthesis via inactivation of NF- κ B pathway in SH-SY5Y cells. *J Biol Res-Thessalon.* 2019;26:15.
76. Krishtal J, Metsla K, Bragina O, Tougu V, Palumaa P. Toxicity of amyloid- β peptides varies depending on differentiation route of SH-SY5Y cells. *J Alzheimers Dis.* 2019;71:879–87.
77. El Kirat K, Burton I, Dupres V, Dufrene YF. Sample preparation procedures for biological atomic force microscopy. *J Microsc-Oxford.* 2005;218:199–207.
78. Deegan RD, Bakajin O, Dupont TF, Huber G, Nagel SR, Witten TA. Capillary flow as the cause of ring stains from dried liquid drops. *Nature.* 1997;389:827–9.
79. Kopecky V, Baumruk V. Structure of the ring in drop coating deposited proteins and its implication for Raman spectroscopy of biomolecules. *Vib Spectrosc.* 2006;42:184–7.
80. Deegan RD. Pattern formation in drying drops. *Phys Rev E.* 2000;61:475–85.
81. Stockert JC, Blázquez-Castro A, Cañete M, Horobin RW, Villanueva A. MTT assay for cell viability: Intracellular localization of the formazan product is in lipid droplets. *Acta Histochem.* 2012;114:785–96.
82. Ozdemir AY, Akbay E, Onur MA. Comparison of the different isoforms of vitamin e against amyloid beta-induced neurodegeneration. *Turk J Biol.* 2022;46:388–99.
83. Kamiloglu S, Sari G, Ozdal T, Capanoglu E. Guidelines for cell viability assays. *Food Front.* 2020;1:332–49.

84. Thammasart S, Namchaiw P, Pasuwat K, Tonsomboon K, Khantachawana A. Attenuation Abeta1-42-induced neurotoxicity in neuronal cell by 660nm and 810nm LED light irradiation. *PLoS ONE*. 2023;18: e0283976.
85. Mali AS, Honc O, Hejnova L, Novotny J. Opioids alleviate oxidative stress via the Nrf2/HO-1 pathway in LPS-stimulated microglia. *Int J Mol Sci*. 2023;24:11089.
86. De Leon JAD, Borges CR. Evaluation of oxidative stress in biological samples using the thiobarbituric acid reactive substances assay. *Jove-J Vis Exp*. 2020;1:61122.
87. Presley AD, Fuller KM, Arriaga EA. MitoTracker green labeling of mitochondrial proteins and their subsequent analysis by capillary electrophoresis with laser-induced fluorescence detection. *J Chromatogr B*. 2003;793:141–50.
88. Monteiro LD, Davanzo GG, de Aguiar CF, Moraes-Vieira PMM. Using flow cytometry for mitochondrial assays. *MethodsX*. 2020;7: 100938.
89. Ip WKE, Hoshi N, Shouval DS, Snapper S, Medzhitov R. Anti-inflammatory effect of IL-10 mediated by metabolic reprogramming of macrophages. *Science*. 2017;356:513–9.
90. Honc O, Novotny J. Methadone potentiates the cytotoxicity of temozolomide by impairing calcium homeostasis and dysregulation of PARP in glioblastoma cells. *Cancers*. 2023;15:3567.
91. Ng KB, Bustamam A, Sukari MA, Abdelwahab SI, Mohan S, Buckle MJC, et al. Induction of selective cytotoxicity and apoptosis in human T4-lymphoblastoid cell line (CEMss) by boesenbergin a isolated from rhizomes involves mitochondrial pathway, activation of caspase 3 and G2/M phase cell cycle arrest. *BMC Complem Altern M*. 2013;13:41.
92. Salim LZA, Mohan S, Othman R, Abdelwahab SI, Kamalidehghan B, Sheikh BY, et al. Thymoquinone induces mitochondria-mediated apoptosis in acute lymphoblastic leukaemia. *Molecules*. 2013;18:11219–40.
93. Bagheri E, Hajiaghaalipour F, Nyamathulla S, Salehen NA. Ethanol extract of inhibit proliferation of HCT-116 colon cancer cells caspase activation. *RSC Adv*. 2018;8:681–9.
94. Martin RM, Leonhardt H, Cardoso MC. DNA labeling in living cells. *Cytom Part A*. 2005;67:45–52.
95. Hu XM, Li ZX, Lin RH, Shan JQ, Yu QW, Wang RX, et al. Guidelines for regulated cell death assays: a systematic summary, a categorical comparison. *Prospect Front Cell Dev Biol*. 2021;9: 634690.
96. Cao Y, Fan MY, Pei YF, Su L, Xiao WW, Chen F, et al. CCAAT/enhancer-binding protein homologous protein (CHOP) deficiency attenuates heatstroke-induced intestinal injury. *Inflammation*. 2022;45:695–711.
97. Cockova Z, Honc O, Telensky P, Olsen MJ, Novotny J. Streptozotocin-induced astrocyte mitochondrial dysfunction is ameliorated by FTO inhibitor MO-I-500. *ACS Chem Neurosci*. 2021;12:3818–28.
98. Lin YC, Komatsu H, Ma J, Axelsen PH, Fakhraai Z. Identifying polymorphs of amyloid-beta (1–42) fibrils using high-resolution atomic force microscopy. *J Phys Chem B*. 2019;123:10376–83.
99. Forster JI, Köglberger S, Trefois C, Boyd O, Baumuratov AS, Buck L, et al. Characterization of differentiated sh-sy5y as neuronal screening model reveals increased oxidative vulnerability. *J Biomol Screen*. 2016;21:496–509.
100. Krishtal J, Bragina O, Metsla K, Palumaa P, Tougu V. In situ fibrillizing amyloid- beta 1–42 induces neurite degeneration and apoptosis of differentiated SH-SY5Y cells. *PLoS ONE*. 2017;12: e0186636.
101. Lopez-Suarez L, Al Awabdh S, Coumoul X, Chauvet C. The SH-SY5Y human neuroblastoma cell line, a relevant in vitro cell model for investigating neurotoxicology in human: Focus on organic pollutants. *Neurotoxicology*. 2022;92:131–55.
102. Qian YH, Xiao QL, Xu J. The protective effects of tanshinone IIA on β -amyloid protein (1–42)-induced cytotoxicity via activation of the Bcl-xL pathway in neuron. *Brain Res Bull*. 2012;88:354–8.
103. Yang SH, Lee DK, Shin J, Lee S, Baek S, Kim J, et al. Nec-1 alleviates cognitive impairment with reduction of Abeta and tau abnormalities in APP/PS1 mice. *EMBO Mol Med*. 2017;9:61–77.
104. Liu WY, Li Y, Li Y, Xu LZ, Jia JP. Carnosic acid attenuates A β O $_2$ -induced apoptosis and synaptic impairment via regulating NMDAR2B and its downstream cascades in SH-SY5Y cells. *Mol Neurobiol*. 2023;60:133–44.
105. Xu SC, Zhong M, Zhang L, Wang Y, Zhou Z, Hao YT, et al. Overexpression of Tfam protects mitochondria against β -amyloid-induced oxidative damage in SH-SY5Y cells. *FEBS J*. 2009;276:4224–33.
106. Du YL, Yang DH, Li L, Luo GR, Li T, Fan XL, et al. An insight into the mechanistic role of p53-mediated autophagy induction in response to proteasomal inhibition-induced neurotoxicity. *Autophagy*. 2009;5:663–75.
107. Radi E, Formichi P, Battisti C, Federico A. Apoptosis and oxidative stress in neurodegenerative diseases. *J Alzheimers Dis*. 2014;42:S125–52.
108. Zhu ZH, Reiser G. The small heat shock proteins, especially HspB4 and HspB5 are promising protectants in neurodegenerative diseases. *Neurochem Int*. 2018;115:69–79.
109. Okle O, Stemmer K, Deschl U, Dietrich DR. BMAA induced ER stress and enhanced caspase 12 cleavage in human neuroblastoma SH-SY5Y cells at low nonexcitotoxic concentrations. *Toxicol Sci*. 2013;131:217–24.
110. Wongprayoon P, Govitrapong P. Melatonin protects SH-SY5Y neuronal cells against methamphetamine-induced endoplasmic reticulum stress and apoptotic cell death. *Neurotox Res*. 2017;31:1–10.
111. Mahaman YAR, Huang F, Kessete Afewerky H, Maibouge TMS, Ghose B, Wang X. Involvement of calpain in the neuropathogenesis of Alzheimer's disease. *Med Res Rev*. 2019;39:608–30.
112. Higuchi M, Iwata N, Matsuba Y, Takano J, Suemoto T, Maeda J, et al. Mechanistic involvement of the calpain-calpastatin system in Alzheimer neuropathology. *FASEB J*. 2012;26:1204–17.
113. Reed T, Perluigi M, Sultana R, Pierce WM, Klein JB, Turner DM, et al. Redox proteomic identification of 4-hydroxy-2-nonenal-modified brain proteins in amnesic mild cognitive impairment: Insight into the role of lipid peroxidation in the progression and pathogenesis of Alzheimer's disease. *Neurobiol Dis*. 2008;30:107–20.
114. Chan HH, Leong CO, Lim CL, Koh RY. Roles of receptor-interacting protein kinase 1 in SH-SY5Y cells with beta amyloid-induced neurotoxicity. *J Cell Mol Med*. 2022;26:1434–44.
115. Abdelhady R, Younis NS, Ali O, Shehata S, Sayed RH, Nadeem RI. Cognitive enhancing effects of pazopanib in D-galactose/ovariectomized Alzheimer's rat model: insights into the role of RIPK1/RIPK3/MLKL necroptosis signaling pathway. *Inflammopharmacology*. 2023;31:2719–29.
116. Sun LM, Wang HY, Wang ZG, He SD, Chen S, Liao DH, et al. Mixed lineage kinase domain-like protein mediates necrosis signaling downstream of RIP3 kinase. *Cell*. 2012;148:213–27.
117. Han CY, Yang Y, Guan QB, Zhang XL, Shen HP, Sheng YJ, et al. New mechanism of nerve injury in Alzheimer's disease: β -amyloid-induced neuronal pyroptosis. *J Cell Mol Med*. 2020;24:8078–90.

118. Tan MA, Ishikawa H, An SSA. Exhibits in vitro anti-amyloidogenic activity and promotes neuroprotective effects in amyloid- β -induced SH-SY5Y Cells. *Nutrients*. 2022;14:3962.
119. Guo YL, Fan ZY, Zhao S, Yu W, Hou XY, Nie SJ, et al. Brain-targeted lycopene-loaded microemulsion modulates neuroinflammation, oxidative stress, apoptosis and synaptic plasticity in β -amyloid-induced Alzheimer's disease mice. *Neurol Res*. 2023;45:753–64.
120. Zhou XP, Tang XM, Li T, Li DD, Gong ZT, Zhang XJ, et al. Inhibition of VDAC1 rescues A-induced mitochondrial dysfunction and ferroptosis via activation of AMPK and Wnt/-Catenin Pathways. *Mediat Inflamm*. 2023;2023:6739691.
121. Kurouski D, Lu XF, Popova L, Wan W, Shanmugasundaram M, Stubbs G, et al. Is Supramolecular filament chirality the underlying cause of major morphology differences in amyloid fibrils? *J Am Chem Soc*. 2014;136:2302–12.
122. Pazderkova M, Pazderka T, Shanmugasundaram M, Dukor RK, Lednev IK, Nafie LA. Origin of enhanced VCD in amyloid fibril spectra: effect of deuteration and pH. *Chirality*. 2017;29:469–75.
123. Wesén E, Jeffries GDM, Dzebo MM, Esbjörner EK. Endocytic uptake of monomeric amyloid- β peptides is clathrin- and dynamin-independent and results in selective accumulation of A β (1–42) compared to A β (1–40). *Sci Rep-Uk*. 2017;7:2021.
124. Morishima Y, Gotoh Y, Zieg J, Barrett T, Takano H, Flavell R, et al. β -amyloid induces neuronal apoptosis via a mechanism that involves the c-Jun N-terminal kinase pathway and the induction of Fas ligand. *J Neurosci*. 2001;21:7551–60.
125. Sharma VK, Singh TG, Singh S, Garg N, Dhiman S. Apoptotic pathways and Alzheimer's disease: probing therapeutic potential. *Neurochem Res*. 2021;46:3103–22.
126. Kole AJ, Annis RP, Deshmukh M. Mature neurons: equipped for survival. *Cell Death Dis*. 2013;4: e689.
127. Hitomi J, Katayama T, Eguchi Y, Kudo T, Taniguchi M, Koyama Y, et al. Involvement of caspase-4 in endoplasmic reticulum stress-induced apoptosis and A β -induced cell death. *J Cell Biol*. 2004;165:347–56.
128. Kam MK, Kim B, Lee DG, Lee HJ, Park YH, Lee DS. Amyloid beta oligomers-induced parkin aggravates ER stress-mediated cell death through a positive feedback loop. *Neurochem Int*. 2022;155: 105312.
129. Hu H, Tian MX, Ding C, Yu SQ. The C/EBP homologous protein (CHOP) transcription factor functions in endoplasmic reticulum stress-induced apoptosis and microbial infection. *Front Immunol*. 2019;9:3083.
130. Zhang FL, Qi Y, Li J, Liu BY, Liu ZH, Cui XL. Activin a induces apoptosis of human lung adenocarcinoma A549 cells through endoplasmic reticulum stress pathway. *Oncol Rep*. 2024;51:29.
131. Esposito L, Raber J, Kekoni L, Yan FR, Yu GQ, Bien-Ly N, et al. Reduction in mitochondrial superoxide dismutase modulates Alzheimer's disease-like pathology and accelerates the onset of behavioral changes in human amyloid precursor protein transgenic mice. *J Neurosci*. 2006;26:5167–79.
132. Fracassi A, Marcatti M, Zolocheska O, Tabor N, Woltjer R, Moreno S, et al. Oxidative damage and antioxidant response in frontal cortex of demented and nondemented individuals with Alzheimer's neuropathology. *J Neurosci*. 2021;41:538–54.
133. Olajide OJ, La Rue C, Bergdahl A, Chapman CA. Inhibiting amyloid beta (1–42) peptide-induced mitochondrial dysfunction prevents the degradation of synaptic proteins in the entorhinal cortex. *Front Aging Neurosci*. 2022;14: 960314.
134. Yoon EJ, Park HJ, Kim GY, Cho HM, Choi JH, Park HY, et al. Intracellular amyloid beta interacts with SOD1 and impairs the enzymatic activity of SOD1: implications for the pathogenesis of amyotrophic lateral sclerosis. *Exp Mol Med*. 2009;41:611–7.
135. Murakami K, Murata N, Noda Y, Tahara S, Kaneko T, Kinoshita N, et al. SOD1 (Copper/Zinc superoxide dismutase) deficiency drives amyloid β protein oligomerization and memory loss in mouse model of Alzheimer disease. *J Biol Chem*. 2011;286:44557–68.
136. Durán-González J, Michi ED, Elorza B, Perez-Córdova MG, Pacheco-Otalora LF, Touhami A, et al. Amyloid β peptides modify the expression of antioxidant repair enzymes and a potassium channel in the septohippocampal system. *Neurobiol Aging*. 2013;34:2071–6.
137. Norambuena A, Sun XH, Wallrabe H, Cao RF, Sun ND, Pardo E, et al. SOD1 mediates lysosome-to-mitochondria communication and its dysregulation by amyloid- β oligomers. *Neurobiol Dis*. 2022;169: 105737.
138. Porcellotti S, Fanelli F, Fracassi A, Sepe S, Ceconi F, Bernardi C, et al. Oxidative stress during the progression of β -amyloid pathology in the neocortex of the Tg2576 mouse model of Alzheimer's disease. *Oxid Med Cell Longev*. 2015;2015: 967203.
139. Ortiz JMP, Swerdlow RH. Mitochondrial dysfunction in Alzheimer's disease: role in pathogenesis and novel therapeutic opportunities. *Br J Pharmacol*. 2019;176:3489–507.
140. Schagger H, Ohm TG. Human-diseases with defects in oxidative-phosphorylation. 2. F1f0 Atp-synthase defects in Alzheimer-disease revealed by blue native polyacrylamide-gel electrophoresis. *Eur J Biochem*. 1995;227:916–21.
141. Terni B, Boada J, Portero-Otin M, Pamplona R, Ferrer I. Mitochondrial ATP-synthase in the entorhinal cortex is a target of oxidative stress at stages I/II of Alzheimer's disease pathology. *Brain Pathol*. 2010;20:222–33.
142. Kunkel GH, Chaturvedi P, Tyagi SC. Mitochondrial pathways to cardiac recovery: TFAM. *Heart Fail Rev*. 2016;21:499–517.
143. Chew K, Zhao L. Interactions of mitochondrial transcription factor a with DNA damage: mechanistic insights and functional implications. *Genes (Basel)*. 2021;12:1246.
144. Zhao M, Wang YZ, Li L, Liu SY, Wang CS, Yuan YJ, et al. Mitochondrial ROS promote mitochondrial dysfunction and inflammation in ischemic acute kidney injury by disrupting TFAM-mediated mtDNA maintenance. *Theranostics*. 2021;11:1845–63.
145. Ho CL, Kao NJ, Lin CI, Cross TWL, Lin SH. Quercetin increases mitochondrial biogenesis and reduces free radicals in neuronal SH-SY5Y Cells. *Nutrients*. 2022;14:3310.
146. Sheng BY, Wang XL, Su B, Lee HG, Casadesus G, Perry G, et al. Impaired mitochondrial biogenesis contributes to mitochondrial dysfunction in Alzheimer's disease. *J Neurochem*. 2012;120:419–29.
147. Aguirre-Rueda D, Guerra-Ojeda S, Aldasoro M, Iradi A, Obrador E, Ortega A, et al. Astrocytes protect neurons from A β peptide-induced neurotoxicity increasing TFAM and PGC-1 and decreasing PPAR- γ and SIRT-1. *Int J Med Sci*. 2015;12:48–56.

148. Ciudad S, Puig E, Botzanowski T, Meigooni M, Arango AS, Do J, et al. A β (1–42) tetramer and octamer structures reveal edge conductivity pores as a mechanism for membrane damage. *Nat Commun.* 2020;11:3014.
149. Song LL, Qu YQ, Tang YP, Chen X, Lo HH, Qu LQ, et al. Hyperoside alleviates toxicity of β -amyloid via endoplasmic reticulum-mitochondrial calcium signal transduction cascade in APP/PS1 double transgenic Alzheimer's disease mice. *Redox Biol.* 2023;61: 102637.
150. Wilhelmus MMM, Boelens WC, Otte-Höller I, Kamps B, de Waal RMW, Verbeek MM. Small heat shock proteins inhibit amyloid- β protein aggregation and cerebrovascular amyloid- β protein toxicity. *Brain Res.* 2006;1089:67–78.
151. Beretta G, Shala AL. Impact of heat shock proteins in neurodegeneration: possible therapeutical targets. *Ann Neurosci.* 2022;29:71–82.
152. Franklin TB, Krueger-Naug AM, Clarke DB, Arrigo AP, Currie RW. The role of heat shock proteins Hsp70 and Hsp27 in cellular protection of the central nervous system. *Int J Hyperther.* 2005;21:379–92.
153. Evans CG, Wisén S, Gestwicki JE. Heat shock proteins 70 and 90 inhibit early stages of amyloid β -(1–42) aggregation. *J Biol Chem.* 2006;281:33182–91.
154. Koper MJ, Van Schoor E, Ospitalieri S, Vandenbergh R, Vandenbulcke M, von Arnim CAF, et al. Necrosome complex detected in granulovacuolar degeneration is associated with neuronal loss in Alzheimer's disease. *Acta Neuropathol.* 2020;139:463–84.
155. Salvadores N, Moreno-Gonzalez I, Gamez N, Quiroz G, Vegas-Gomez L, Escandón M, et al. A β oligomers trigger necroptosis-mediated neurodegeneration via microglia activation in Alzheimer's disease. *Acta Neuropathol Commun.* 2022;10:31.
156. Hernández DE, Salvadores NA, Moya-Alvarado G, Catalán RJ, Bronfman FC, Court FA. Axonal degeneration induced by glutamate excitotoxicity is mediated by necroptosis. *J Cell Sci.* 2018;131:214684.
157. Arrázola MS, Saquel C, Catalán RJ, Barrientos SA, Hernandez DE, Martínez NW, et al. Axonal degeneration is mediated by necroptosis activation. *J Neurosci.* 2019;39:3832–44.
158. Kakio A, Nishimoto S, Yanagisawa K, Kozutsumi Y, Matsuzaki K. Interactions of amyloid β -protein with various gangliosides in raft-like membranes: importance of GM1 ganglioside-bound form as an endogenous seed for Alzheimer amyloid. *Biochemistry US.* 2002;41:7385–90.
159. Yanagisawa M, Ariga T, Yu RK. Cytotoxic effects of G(M1) ganglioside and amyloid beta-peptide on mouse embryonic neural stem cells. *ASN Neuro.* 2010;2: e00029.
160. Nicastro MC, Spigolon D, Librizzi F, Moran O, Ortore MG, Bulone D, et al. Amyloid β -peptide insertion in liposomes containing GM1-cholesterol domains. *Biophys Chem.* 2016;208:9–16.
161. Matsubara T, Nishihara M, Yasumori H, Nakai M, Yanagisawa K, Sato T. Size and shape of amyloid fibrils induced by ganglioside nanoclusters: role of sialyl oligosaccharide in fibril formation. *Langmuir.* 2017;33:13874–81.
162. Ahyayauch H, de la Arada I, Masserini ME, Arrondo JLR, Goñi FM, Alonso A. The binding of A β 42 peptide monomers to sphingomyelin/cholesterol/ganglioside bilayers assayed by density gradient ultracentrifugation. *Int J Mol Sci.* 2020;21:1674.
163. Matsuzaki K. Abeta-ganglioside interactions in the pathogenesis of Alzheimer's disease. *Biochim Biophys Acta Biomembr.* 2020;1862: 183233.
164. Jiang L, Bechtel MD, Bean JL, Winefield R, Williams TD, Zaidi A, et al. Effects of gangliosides on the activity of the plasma membrane Ca-ATPase. *BBA Biomembranes.* 2014;1838:1255–65.
165. Amaro M, Sachl R, Aydogan G, Mikhalyov II, Vácha R, Hof M. GM ganglioside Inhibits β -amyloid oligomerization induced by sphingomyelin. *Angew Chem Int Edit.* 2016;55:9411–5.
166. Owen MC, Kulig W, Poojari C, Rog T, Strodel B. Physiologically-relevant levels of sphingomyelin, but not GM1, induces a beta-sheet-rich structure in the amyloid-beta(1–42) monomer. *Biochim Biophys Acta Biomembr.* 2018;1860:1709–20.
167. Carrotta R, Mangione MR, Librizzi F, Moran O. Small Angle X-ray scattering sensing membrane composition: the role of sphingolipids in membrane-amyloid β -peptide interaction. *Biology (Basel).* 2022;11:26.

Publisher's Note

Springer Nature remains neutral with regard to jurisdictional claims in published maps and institutional affiliations.